Temperature-dependent predation predicts a more reptilian future

Author names and affiliations:

John M. Grady[1,2,3*†], Jacob L. Amme[2*], Kiran Bhaskaran-Nair[2], Varun Sinha[2], Samuel J. Brunwasser[2], Sydne Record[3], Anthony I. Dell[1,4‡], Keith B. Hengen[2‡†]

[1]Living Earth Collaborative Center for Biodiversity, Washington University in Saint Louis, St. Louis, MO, USA [2]Department of Biology, Washington University in Saint Louis, St. Louis, MO, USA [3] Department of Wildlife, Fisheries, and Conservation Biology, University of Maine, Orono, ME, USA [4] National Great Rivers Research and Education Center, East Alton IL, USA

[*]These authors contributed equally to this work.

[‡]Last author

[†]Corresponding author: jgradym@gmail.com, khengen@wustl.edu

Abstract

Diversity increases toward the tropics, but the strength of this pattern diverges with thermoregulatory strategy. Synthesizing over 30,000 species distributions, we quantified patterns of richness in terrestrial vertebrates, and present evidence for a latitudinal gradient of community composition. We observe a two orders of magnitude shift in comparative diversity with temperature, from endothermic mammal and avian dominance near the poles, toward ectothermic reptile and amphibian majority in the tropics. Next, we provide mechanistic support for a corresponding latitudinal gradient of predatory interactions. Using automated video tracking in >4500 trials, we show that differences in thermal sensitivity of locomotion in endothermic predators and ectothermic prey favors endotherms in colder environments and yields theoretically predicted foraging outcomes across thermal conditions, including the number of strikes, the distance traveled, and the time to capture prey. We also present evidence that endotherms use thermal cues to anticipate prey behavior, modulating the impact of temperature. Finally, we integrate theory and data to forecast future patterns of diversity, revealing that as the world get warmer, it will become increasingly reptilian. Overall, our results point toward a broad reorganization of vertebrate diversity with latitude, elevation, and temperature: from endotherm dominance in cold systems toward ectotherm dominance in warm.

Introduction

One of the most widely recognized patterns in ecology is that species richness increases toward the tropics, known as the latitudinal diversity gradient[1,2]. Temperature also increases toward the tropics, and how temperature influences richness has generated considerable debate[3]. Allen et al. (2002)[4] demonstrated that the richness of 'cold-blooded' ectotherms, like reptiles and invertebrates, increased with ambient temperature at rates similar to their metabolism, suggesting deep linkages between physiology and species diversity (see also[5–8]). Specifically, they showed that both metabolic rate B and richness R show the same temperature dependence for many taxa:

$$B \propto R \propto e^{-E/kT} \tag{1}$$

where $\propto$ indicates proportionality, k is Boltzmann's constant, T is temperature in Kelvins and E is a thermal sensitivity coefficient ('activation energy') that is ~ 0.65 for metabolic rate[9], corresponding to ~ 2.5 fold increase per 10 °C (i.e., $Q_{10} = 2.5$).

Not all animals are ectothermic, however. Among vertebrates, the majority are 'warm-blooded' endotherms, i.e., mammals or birds that use metabolic heat to maintain a constant internal body temperature. While all major endothermic and ectothermic taxa have higher diversity in the tropics[2], it is less appreciated that spatial patterns of endotherm and ectotherm diversity are quite different. Consistent with their stable body temperature, evidence is accumulating that the richness of mammals and birds shows a much weaker temperature dependence than ectotherms[4,7]. An important implication of these findings is that ectotherms should be comparatively more speciose than endotherms toward the tropics, generating a latitudinal gradient in the composition of vertebrate communities.

To assess this prediction, we synthesized the most extensive dataset of terrestrial vertebrate diversity to date — spanning 30,859 species distributions of reptiles, amphibians, mammals, and birds — and quantified comparative patterns of diversity in endotherms and ectotherms. Distributional maps are often used to calculate regional richness, but because regional and local richness are closely linked[10–12], they are also useful for approximating the local richness of communities. We used the ratio of endotherm to ectotherm richness as a metric for relative composition, and regressed this against surface temperature, with precipitation and elevation as covariates (Fig. 1). Although richness in all major vertebrate taxa show a positive association with temperature, the comparative patterns are much more divergent (Fig. 1; Figs. S1-S2). We observe a 85-fold shift in relative richness with temperature globally, with over 190 times more mammals and bird species in the coldest habitats relative to ectotherms, but only 2.3 times as many in the warmest. The magnitude of this compositional shift is nearly equivalent to the thermal sensitivity of metabolic rate, with an a 2.2-fold increase in relative richness per 10 °C (Fig. 1, linear mixed model: $E = 0.57$, $CI : 0.57 - 0.58$ for all vertebrates, $r^2 = 0.76$; spatial Bayesian hierarchical model: $E = 0.66$, $CI = 0.66 - 0.67$, $r^2 = 0.98$; see also Table S1). This thermally mediated shift not only occurs with latitude but elevation as well (Fig. S3), as illustrated by the red spike in relative endotherm diversity in the Himalayas and Rocky Mountains (Fig. 1A).

A Latidudinal Gradient of Predatory Interactions Not only are endotherms comparatively more speciose in colder habitats, evidence is accumulating that they are more abundant as well. In the ocean, a thermal gradient of comparative richness, abundance, and energy flow has been documented across the globe, from large, predatory ectothermic fish in the tropics, to endothermic whales, seals, and birds toward the poles[13,14]. On land, a global synthesis of vertebrate abundance by Santini et al. (2018)[15] found mammal abundance to be highest in temperate areas, while reptiles are higher in the tropics. This gradient extends to trophic interactions, which

are widespread between endotherms and ectotherms: the majority of all mammals and birds, for instance, include invertebrates in their diet[16,17]. Using a experimental approach at a global scale, Roslin et al. (2017)[18] observed that the frequency of attack on insects by arthropods increased toward the lowland tropics but attack rates from mammal and birds on insects were invariant. Thus, the proportion of attacks by endotherms rose in high latitudes and elevations. Collectively, these results point toward a corresponding latitudinal gradient of predatory interactions between endotherms and ectotherms that tracks gradients in species diversity.

Testing Theoretical Mechanisms What is the mechanism behind this latitudinal gradient in predatory interactions? One hypothesis is that with endotherms becoming progressively better predators in high latitudes because their ectothermic prey are colder and more sluggish[13,14]. This idea was formalized in Grady et al. (2019) as Metabolic Asymmetry Theory (MAT), which accurately predicted ecosystem-scale patterns of consumption in marine mammals based on the asymmetry in thermal performance relative to ectothermic prey and competitors: bony fish and sharks[14]. At the scale of individual interactions, a key assumption of MAT is that the difference in thermal sensitivities of reaction times and locomotory rates like speed S predict predatory outcomes, such as the probability of an ectothermic prey escaping:

$$P(Escape) \propto \Delta S \propto e^{-E/kT} \tag{2}$$

where $\Delta S \equiv S_{\text{Ecto}}/S_{\text{Endo}}$. If correct, this would provide a simple, quantitative mechanism behind the observed spatial gradient in endotherm/ectotherm diversity. However, this prediction has not been experimentally tested. Indeed, previous thermal assessments of endo/ecto predation are generally limited to passive consumption of slow-moving prey (see references in[19].) More broadly, metabolic-based theories in ecology have been criticized for lacking mechanistic validation[20]. Unlike particles blindly colliding in space, predator and prey interactions involve nonrandom patterns of pursuit and escape that can dampen or exacerbate metabolic effects. Predators often exhibit behavioral plasticity while foraging, further regulating physiological constraints. Thus, it is unclear how closely biotic interactions track differences in metabolism with temperature. To determine whether pursuit-based predation truly reflects temperature and theory, controlled experiments are needed.

To test MAT and evaluate the effects of temperature on endotherm/ectotherm predation, we manipulated ambient temperature and quantified pursuit and capture rates between an endothermic predator, the laboratory mouse (*Mus musculus*), and an ectothermic prey, the fast-moving, red runner cockroach (*Periplaneta lateralis*). In nature, rodents are opportunistic predators of ectothermic invertebrates, and research shows that even inbred laboratory mice with no prior hunting experience quickly learn to pursue and capture insects[21–24]. We trained C57BL/6 laboratory mice to hunt red runners at room temperature and then performed 4,747 individual foraging trials at five temperatures, ranging from 14 to 35 °C (Fig. 2). We assessed predator and prey movement using video tracking and markerless pose estimation with deep learning, and assessed the theoretical predictions of MAT at three, interconnected levels: i) locomotion in isolation, ii) locomotion during pursuit/escape, and iii) foraging outcomes (Fig. 2A-C, Fig. 3). Next, we tested a secondary assumption of MAT — that predator learning can modulate thermal constraints on prey capture — and present evidence that mice use ambient temperature directly to predict prey behavior during hunting. Finally, we integrate theory and empirical patterns of diversity to forecast shifts in richness under multiple warming scenarios.

Experimental Results

Training Mice to Hunt Mice first learned to hunt during the initial trial stage, which spanned two weeks. Initial hunting trials were conducted at room temperature (25 °C), following overnight food restriction. On each day of trials, up to six red runners were sequentially introduced to each mouse, with a 10 minute delay between prey introductions (Fig. 2D). Analysis of the video of each foraging trial revealed that all mice rapidly learned to hunt red runners: the average time to capture declined from 331 s on the first day, to 29 s by the sixth day (Fig. 3D, Fig. S4), stabilizing at 18 s after two weeks of initial trials. While foraging, a strike was recorded when the mouse was close enough to occlude the red runner from overhead view (Fig. 3B-C). Prey capture involved multiple strikes that iteratively damaged a prey, which was considered captured when it could no longer move away from the mouse. It was typically consumed shortly afterward.

Thermal Asymmetry of Locomotion We assessed mouse and red runner locomotion at different temperatures in isolation and tested model predictions (Fig. 2A-C). As expected, red runner body temperature directly tracked ambient temperature that ranged from 14 to 35 °C, while mouse body temperature was invariant (Fig. S5A-B). We predicted that mouse speed and acceleration in isolation would be invariant with temperature ($E = 0$), while red runners would increase ∼exponentially until a peak, following $Eq.1$. Across ectothermic species, the thermal sensitivity coefficient E has been found to be ~ 0.65 for respiration[9]. In a synthesis of the thermal movement literature, Dell et al. (2011) found a slightly lower value for speed, with an average of $E = 0.51$ ($Q_{10} = 2$)[25]. Thus, for red runner locomotion we predicted $E = 0.5 - 0.65$. To calculate E, we used a mixed model linear regression, where temperature and red runner mass are predictor variables, E is the slope, and mouse ID is a random effect (Fig. S6). Because red runner speeds typically peaked at 30 °C, we restricted regression fits to predation trials ranging from 14–30 °C (solid lines; Fig. 4), but we also plot generalized additive model fits to show the full range of performance at all temperatures (dashed lines; Fig. 4).

Consistent with expectations (Fig. 4A), mouse speed and acceleration in isolation showed little effect of temperature (Fig. 4B, $E_{SpeedMouse} = -0.0086$, confidence interval (CI): $-0.017, -0.00014$; $E_{AccMouse} = -0.00048$, CI: $-0.0072, 0.0063$; see also Table 1); while red runner speed was thermally dependent and near the predicted range (Fig. 4C, $E_{SpeedRRunner} = 0.42$, CI: $0.38, 0.46$), though the thermal dependence of acceleration was lower than expected ($E_{AccRRunner} = 0.14$, CI: $0.13, 0.15$; see also Table 1). Instantaneous, frame-to-frame locomotory rates also showed the same qualitative pattern, with the range and central tendency of distributions shifting toward higher values for red runners at warmer temperatures, but invariant for mice (Figs. S5C,D, S7). Note, all reported E values are for median rates, but E values for maximum rates are similar (Table 1).

Predation Across Temperatures Next, we conducted hunting trials at different temperatures following the same protocol. Similar to rates of movement in isolation, we predicted an approximately exponential increase in locomotion for red runners during pursuit until reaching a peak. However, for mice hunting red runners, mice were expected to show a positive but flatter response to temperature. ($0 < E_{Mouse} < E_{RedRunner}$; Fig. 4D). Results supported predictions, with red runner speed increasing rapidly until reaching a plateau at 30 °C ($E_{SpeedRRunner} = 0.56$; CI: $0.53, 0.60$), while mice likewise had a positive but weaker thermal sensitivity during pursuit ($E_{SpeedMouse} = 0.16$, CI: $0.15 - 0.17$ (Fig. 4E-F; Fig. S8). The thermal sensitivity for red runner acceleration was lower than speed ($E_{Accel} = 0.19$, CI: $0.17, 0.21$), though maximum rates were higher (Table 1.)

A key prediction of MAT is that the difference in thermal sensitivity of locomotion between a predator and its prey ($Eq.2$) predicts the probability of escape. The thermal sensitivity of

$S_{\mathrm{Ecto}}/S_{\mathrm{Endo}}$ is equivalent to $E_{\mathrm{Ecto}} - E_{\mathrm{Endo}} \equiv \Delta E$. Given that red runners were unable to exit the arena, we used time to capture as a proxy for probability of escape, since longer times of pursuit increase the likelihood that a prey finds refuge or outpaces its pursuer in nature. To predict the thermal sensitivity of time to capture ($E_{CaptureTime}$), we used two measures of ΔE_{Speed} observed in isolation — median speed and maximum speed — since both estimates of ΔE_{Speed} are likely relevant to predation (Fig. 4B-C; Table 1). Since the observed ΔE_{Speed} ranged from $0.43 - 0.67$, we predicted that $E_{CaptureTime}$ would fall within this range (Fig. 4G). Consistent with our prediction, $E_{CaptureTime} = 0.51$ (CI: $0.47, 0.55$, $r^2 = 0.56$; Fig. 4I; Table 1). Thus, we find support for the core MAT prediction that differences in thermal sensitivity drive the probability of escape.

In addition, we found that $E_{CaptureTime}$ was comparable in magnitude to the thermal sensitivity of strikes required to subdue prey: $E_{Strikes} = 0.42$ (CI: $0.38, 0.47$; Fig. 4H). This provides mechanistic insight into how differences in thermal sensitivities translate into longer capture times. In particular, the difficulty for a predator in capturing prey at higher temperatures is not merely catching up to them, but also involves the challenges of subduing metabolically active prey, which required more strikes to incapacitate. Note that all patterns in thermal trials hold not only for pooled data (Fig. 4), but also for individual mice (Fig. S9).

Learning to Hunt: Integrating the Components of Hunting

Pursue Results from our hunting trials can be integrated to form a more holistic view of how temperature shapes active-capture predation in endotherms and ectotherms (Fig. 5). First, mice learn to pursue prey by increasing their own speed and maintaining a close proximity to prey (Fig. 5A,C). In our initial trials, mouse speed increased from 13 to 17 cm/s , as the average distance to prey declined from 14 to 4 cm. Hunting at different temperatures merely shifted mouse speed up or down, as it tracks prey speed (Fig. 5D). By keeping pace with prey, mice maintained a constant average distance from red runners irrespective of temperature (Fig. 5B; $p = 0.09$, $n = 1332$ trials).

Strike Next, mice learned to strike repeatedly until prey were subdued (Fig. 5E,G). In initial trials, strike rate increased from once per 17 seconds to once every 3 seconds (Fig. 5E). Efficiency also increased, with the strikes needed to subdue prey declining from 20 per trial to 5 per trial by the close of the initial training period (Fig. 5G). By keeping a constant distance from prey at all temperatures (Fig. 5B), mice maintained an invariant strike frequency over thermal conditions: no difference was detected across temperatures (Fig. 5F; $p = 0.11$).

Capture Finally, mice must incapacitate and capture prey to consume them. Mice showed rapid improvement in the time and distance required to capture prey (Fig. 5I,K), declining from 331 s to 12 s to capture, and from 632 cm traveled in pursuit to 79 cm. A constant strike rate of every three seconds multiplied by higher total strikes required at warmer temperatures yielded longer pursuit times as temperatures rose (Fig. 5F,H,J). The distance traveled per capture also increased with temperature, but at higher rates ($E_{CaptureDistance} = 1.1$, CI: 1.0–1.1, vs $E_{CaptureTime} = 0.51$; Fig. 5L, Table 1). This can be understood by considering that distance is the product of speed and time, so the thermal sensitivity of distance traveled is greater than its components.

Together, these elements of hunting show a strong signature of learning that is most pronounced during the initial trial phase at room temperature, where all slopes of hunting performance with trial number are significantly different than zero (Fig. 5; $p < 0.001$ and $r^2 \geq 0.3$ for all). Performance differences between 30 and 35 °C were typically non-significant; otherwise significant differences in mean performance across different temperatures were noted in all trials, with the exception of average distance between predator and prey and strike rate, which were both thermally invariant (Fig. 5B,F)).

Using Temperature to Adapt Hunting Strategy Adapting hunting strategy is a potential way for endotherms to mitigate the kinetic challenges of capturing ectotherms at warm temperatures. In the context of our predator-prey experiment, we consider two scenarios by which endothermic mice learn to hunt across a thermal gradient. The first possibility is the simplest; mice tailor aspects of hunting behavior to the locomotion of prey, e.g., speeding up to chase warmer, faster red runners, and slowing down to capture cold, sluggish prey. Alternatively, mice may also engage in behavioral forecasting, using ambient temperature to predict the behavior of prey.

After the conclusion of thermal trials, we designed an experiment to test these scenarios by violating the potential expectations of the mice. In a typical hunting trial, ambient arena temperature is the same for mice and red runners. Thus a hot arena predicts a hot, fast prey and cold arena predicts a cold, slow prey. At the conclusion of thermal trials, each mouse had undergone hundreds of paired trials in total, spanning all tested temperatures. Subsequently, by occasionally breaking this association — i.e., delivering a warm prey to a cold arena or a cold prey to a warm arena — we assessed whether violating the mouse's potential expectations of prey behavior on the basis of temperature altered performance. To maintain the any learned associations, these "mismatch" trials only occurred once every other day on the first of six daily trials, over the course of 12 days. We then compared hunting performance during a thermal mismatch to the first daily trial at standard hunting conditions (Fig. 6) — i.e., cold prey under standard cold conditions vs cold prey in mismatched conditions, and again for warm conditions.

Given the short duration of pursuit in a typical trial, mismatched prey did not cool or warm in arenas sufficiently quickly to significantly alter speed and acceleration from standard conditions (Fig. 6B,D; Fig. S10; $p > 0.05$), nor did mouse speed and acceleration change in mismatched conditions (Fig. 6B,D; $p > 0.3$). This indicates that predator and prey locomotion in standard and mismatch scenarios were fundamentally similar, and that differences in predation outcomes, if observed, reflect behavioral shifts in mice. For performance variables where we previously observed mice to be thermally insensitive — distance to prey and strike rate (Fig. 5B,F) — no effect of mismatch was expected or observed (Fig. 6B,D shaded gray). However, for all conditions where temperature affects performance, mismatch conditions led to significantly different foraging outcomes. For example, for mice receiving cold prey in warm arenas ('cold mismatch'), strikes per capture, time per capture, and distance traveled per capture were all significantly higher than standard cold conditions where both prey and arenas were cold, with large effect sizes (Fig. 6A,B; all $p < 0.01$ and Cohen's d > 1.4; see also Table S2). In 'warm mismatch' conditions (warm prey, cold arena), differences in strikes per capture was near significance compared to standard warm conditions ($p = 0.056$), while time to capture, and distance to capture varied significantly, with medium to large effect sizes (Fig. 6C,D; $p < 0.01$, d < -0.78; see also Table S2). Interestingly, in the warm mismatch experiment (Fig. 6C,D), the direction of the change was opposite of what was expected: mice performed better at capturing warm prey in cold arenas than in warm arenas. Even if not perfectly adaptive, these findings represent, to our knowledge, the first experimental evidence that endothermic predators learn to use thermal cues to anticipate prey behavior.

Forecasting Global Vertebrate Diversity Under Warming Conditions Both theory and data indicate that as temperatures warm, endothermic predators will face increasing challenges in capturing ectothermic prey. This may lead to compositional shifts due to disproportionate attrition of endotherms and/or expansion of ectotherms in warmer habitats. If such trends are sustained, we predict this will eventually lead to relatively higher occupancy, abundance, and diversity of ectothermic vertebrates as pressure from endothermic predators and competitors declines.

To forecast how the relative balance of endotherms and ectotherms will change under warming

scenarios, we use CMIP 6 climate change scenarios for 2100 adopted by the Intergovernmental Panel on Climate Change[26,27], including a optimistic scenario of a global 1.4 °C increase[28], a more realistic 2.6 °C increase[29], and a high, "business as usual" approach leading to increase of global increase of 5.4 °C[30]. In projecting how the relative balance of endotherms and ectotherms will change under these different scenarios, we focus on mammals and reptiles, which are both primarily terrestrial, quadrupedal, and are not reproductively tied to water. In Fig. 7, red color indicates more mammals than reptiles, conversely blue indicates more reptiles. Mammals are more speciose than reptiles on 66% of the earth's surface today where both coexist (mean ratio = 6.5, SD = 3.0). Under a 1.5 °C increase that percentage declined to 56%, at 2.6 °C it declined to 49%. With a 5.4 °C increase, the pattern was reversed: mammals were only more speciose in 38% (mean ratio = 3.8, SD = 3.0). A interesting secondary pattern relates to water precipitation: reptile richness (dominated by squamates) increases proportionally more than mammals in dry habitats (y = -0.24 - 0.084(temperature) + 0.11log(annual precipitation); all variables; $p < 0.001$). This effect is modest compared to temperature (temperature partial $r^2 = 0.68$, precipitation partial $r^2 = 0.014$). For example, two areas of the highest proportional reptilian diversity are the Sahara desert and the arid interior of Australia (Fig. 7). This may reflect the lower metabolic demands of reptiles, permitting greater occupancy of unproductive deserts. Overall, our results indicate that as the earth warms, hot and dry areas are expected to see the greatest proportional increase in reptile diversity.

Discussion

It is long been recognized that diversity increases toward the tropics, a pattern known as the latitudinal diversity gradient. Ambient temperature declines with increases in latitude and, indeed, temperature appears to be the single best environmental predictor of richness for many taxa[4,31]. If this role is causal at a physiological level, thermoregulatory strategy — which determines internal body temperature — should be an equally strong predictor of vertebrate diversity. In particular, warm-bodied endotherms should be relatively more diverse in colder, higher latitudes, leading to strong shifts in comparative diversity and community composition as a function of temperature. Supporting this prediction, the relative richness of vertebrate endotherms and ectotherms varied systematically with temperature, from endotherm-dominance in high latitudes and elevations toward ectotherm dominance in the lowland tropics (Fig. 1; Fig. S1-S3). Strikingly, the magnitude of the shift in relative diversity is almost identical to the thermal sensitivity of metabolic rates, supporting theoretical arguments that metabolism is a structuring force of global diversity[4,6,14].

The recognition of a latitudinal gradient of species diversity has inspired a search for a comparable latitudinal gradient in species interactions[32]. One theorized pattern is a gradient in predatory interactions between endotherms and ectotherms, whereby endothermic predators have foraging and competitive advantages in higher latitudes[13,14]. Grady et al. (2019)[14] provided quantitative, ecosystem-scale support in the ocean for this gradient, while Roslin et al. (2017)[18] used field experiments to establish a similar pattern on land. Until now, however, no mechanism underlying this gradient has not been convincingly established. Here we provide a proof-of-concept support that temperature causally favors endothermic predators in cold environments, and ectothermic prey in warm environments. Using over 4500 foraging trials of predatory mice and insect prey, we demonstrate that the thermal sensitivity of time to capture and strikes required per capture closely matches the difference in thermal sensitivity of speed between the endothermic predator and its ectothermic prey (Figs. 4,5). In particular, red runner speed approximately doubles every 10 °C, corresponding to a doubling of the number of strikes and time required for endothermic mice to subdue prey. These results support a key prediction of Metabolic Asymmetry Theory (MAT)[14] :

that the probability of capture is a function of thermal performance asymmetries between predator and prey. It also adds to a growing body of evidence that biotic interactions shift with latitude[18,33], shaping the geographical distribution of terrestrial vertebrates[34].

A secondary prediction of MAT is that learning and behavioral adaptation may help mitigate the kinetic challenges of hunting at warm temperatures[14]. We present evidence that mice directly use thermal cues in the environment to anticipate and adjust to prey behavior at different temperature (Fig. 6). After running thousands of trials where hunting arena temperature and prey temperature were paired, we occasionally broke this pairing and then compared hunting rates between trials where mice received prey with a body temperature matching arena temperature and trials where they did not (thermal mismatch). When a thermal mismatch occurred, key components of mouse foraging change significantly — including the time, distance, and strikes required to capture prey — even though prey temperature and locomotory rates of both predator and prey remained unchanged. These results suggest that while temperature places constraints on endotherm–ectotherm interactions, behavioral responses can mitigate some kinetic challenges.

In nature, the effects of learning and behavioral adaptation may be even more pronounced. For examples, agamid lizards flee from predators at warmer temperatures, but choose to fight at colder temperatures, likely reflecting their relative inability to escape when their body temperatures are low[35]. Similarly, the distance at which an Anolis lizard flees a predator is temperature dependent: at colder temperatures it initiates flight at a further distance[36]. As ocean temperature warm toward the tropics, the disappearance of solitary penguins and seals and the dominance of intelligent, cooperatively foraging dolphins may reflect the challenges of dealing with warm, fast-moving fish[14]. Extending this further, the ultimate intelligent, social predator – humans – use hooks, nets, and radar to capture fish at any speed, insulating us from the negative effects of temperature on food extraction.

How Temperature Shapes Richness After establishing that temperature shapes predatory interactions between endotherms and ectotherms, we considered how thermal asymmetries scale up to influence species richness and the organization of entire communities. First, the challenges of capturing fast-moving ectothermic prey in warm conditions may lead to decreased densities and niche opportunities for endothermic mammals and birds that feed on ectotherms. Indeed, such differences in population density have been recently noted on both land and ocean[14,15]. This limits the occurrence and richness of endotherms in the tropics, but opens opportunities for endothermic predators in cold habitats, where they are comparatively more efficient hunters. For instance, one of the largest families of invertebrate-hunting mammals, shrews (Soricidae; $>$ 230 spp), are diverse in the temperate northern hemisphere, but effectively absent from the lowland neotropics (subfamily Soricinae in Fig S11A), where invertebrates are plentiful but also warm and fast[37]. Only by depressing their metabolism and food requirements to half of their New World relatives[38], do Old World shrews (Crocidurinae) claim this habitat in tropical Africa and Asia (Fig. S11B).

Conversely, ectotherms are at greater risk of predation at high latitudes and elevations, which may lead to range reduction, local extinction, and a loss of realized niches. We suggest this is especially true for large ectotherms, which have more limited opportunities to hide and avoid detection — an effective low-energy approach to predation. This may be an important factor in why endotherms tend to follow Bergmann's rule in having larger body sizes in cold habitats[39], but ectothermic vertebrates do not[40]. These constraints not only apply to ectothermic prey, but also to ectothermic predators. Ectothermic hunters of endotherms are relatively rare. Among those that exist, such as snakes and crocodilians, they seldom pursue endothermic prey but instead rely on surprise to ambush their prey. Indeed, despite a wide occurrence in the geological past,

ectotherm diversity at large body sizes is notably rare today[41]. Giant, slow-metabolizing reptiles and synapsids wandered across Permian and Triassic landscapes, but it is unlikely that buffalo-sized iguanas, for instance, could survive the perils of warm-blooded lions today. Over time, biotic constraints imposed by endotherms have closed niche opportunities for large ectotherms.

Temperature Reorganizes Communities Shifting patterns of endotherm and ectotherm composition may change the structure of ecosystems across time and space. In the ocean, the relative abundance and energy flow toward marine endotherms at high latitudes increase even faster than richness[14]. On land, our experimental findings on temperature-dependent predation coupled with surveys of vertebrate abundance and predation frequency[15,18] indicate that both the frequency and strength of interactions between endotherms and ectotherm shift directionally with temperature. The consequence is a global reorganization of vertebrate diversity with latitude and elevation: from endotherm-dominant in cold systems to ectotherm parity in warm systems. Recent work on bird nestling predation supports this shift. In the tropics, predation of tropical bird nestlings by reptiles declines with elevation, while mammal predation increases[42] . Further, the disproportionate increase of reptiles in dry areas relative to mammals points toward an additional theme: the value of high metabolic rate depends on resource availability. Endotherms may have advantages over ectotherms with respect to locomotory rates and reaction times, among other things, but the cost is an order of magnitude more food consumption. In low resource environments like deserts, the balance may tip toward the low-energy strategy of reptiles.

Conversely, other elements of endotherm/ectotherm composition with temperature may stabilize ecosystem structure across latitude. In an "energy equivalence" world (*sensu*[4,43]), an increase in individual metabolism with temperature is expected to generate lower ectothermic densities and biomass in the tropics, since each individual requires more resources to sustain a high metabolism. Today, however, vertebrate communities are characterized by a transition from warm ectotherms in the tropics to warm endotherms in high latitudes. Warm body temperatures and high metabolism at all latitudes helps equalize per capita energy use, vertebrate biomass, and population density over space.

The Future of Vertebrate Diversity Our work here contributes to an accumulating body of evidence that biotic interactions are major drivers of the geographical distribution of vertebrates, particularly in warm environments[34]. Climate models indicate the world will continue to warm from ongoing carbon emissions. By integrating theory and data, we are now in position to forecast how the composition of vertebrates will change as Earth's climate warms. Under three CMIP6 projections[26,27,29,30], we found that mammal richness compared to reptiles declined from two thirds majority of the earth's surface, to nearly the inverse at a 6.4 °C projected temperature increase. Thus, continued warming of Earth's climate will not only influence the fortunes of individual species, it will also lead to predictable changes in the composition and structure of entire ecosystems.

We expect that as global temperature rise, patterns of energy flow and relative richness will increasingly favor ectothermic invertebrates, reptiles, and fish. Because richness reflects longer, macroevolutionary processess like speciation, shifts in species number may not be immediately observed, but instead represent an equilibrium state that ecological communities will move toward. Over the short term, changes in comparative abundance are predicted to occur first, with a greater attrition of mammal or birds than reptiles, or at least lower comparative rates of increase. This may be particularly true for endotherms feeding on agile, ectothermic prey, such as small, invertivorous mammals and birds on land, and piscivorous pinnipeds and penguins at sea. Conversely, other groups should be less affected, including cognitively flexible predators like dolphins, or groups where no metabolic asymmetry is present, such as endothermic herbivores and their warm-blooded

predators. Nonetheless, a broad, proportional decline in endotherm composition and abundance in a warming world should create more opportunities for invertebrates, reptiles, and fish. Climate change imposes constraints on all animals but the effects of hotter temperatures will not be distributed equally, and we expect the future of life on land to become increasingly reptilian.

Acknowledgments

This project was supported by Living Earth Collaborative at Washington University in St. Louis (J.M.G.). J.M.G. and A.I.D. were supported by a National Science Foundation grant DEB-1838346. Support was also provided by the National Institutes of Health BRAIN (Brain Research through Advancing Innovative Neurotechnologies) Initiative award R01NS118442 (K.B.H.), the National Institutes of Health, Institutional national research service award T32EY013360, and from the National Eye Institute (J.L.A). We thank Michael Moore and James Stroud for helpful suggestions, and Marcos Bermudez and Nicole Paquette for assistance running experiments.

Figures

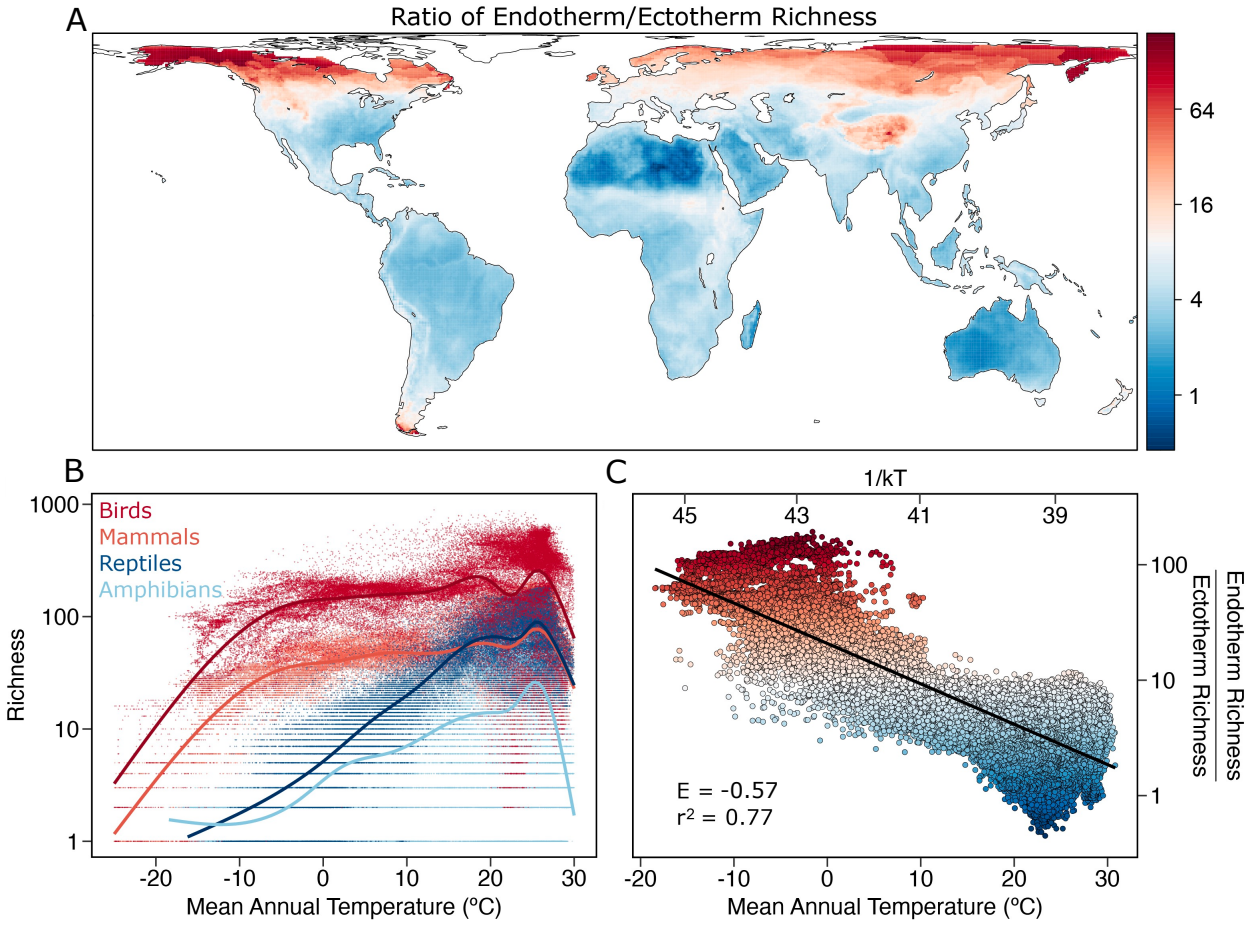

Figure 1: Global patterns of diversity in terrestrial endotherms and ectotherms. **(A)** Endotherms are proportionally more diverse than ectotherms in higher latitudes, generating a latitudinal gradient in the composition of vertebrate communities. **(B)** All major taxa of vertebrates show nonlinear increase in diversity toward the tropics, but ectothermic amphibians and reptiles show a much steeper increase than mammals or birds. **(C)** Ratio values from (A) are plotted against temperature, revealing an approximately linear decline in comparative endotherm/ectotherm richness with surface temperature, where the slope is indicated by the thermal sensitivity coefficient E. Note the rate of decline in relative richness (linear model: E = -0.57; spatial model: E = -0.66) is almost identical in magnitude to the thermal sensitivity of metabolism (E = 0.65), suggesting that metabolic differences in thermal sensitivity underly global variation in vertebrate diversity. See also Figs. S1, S2.

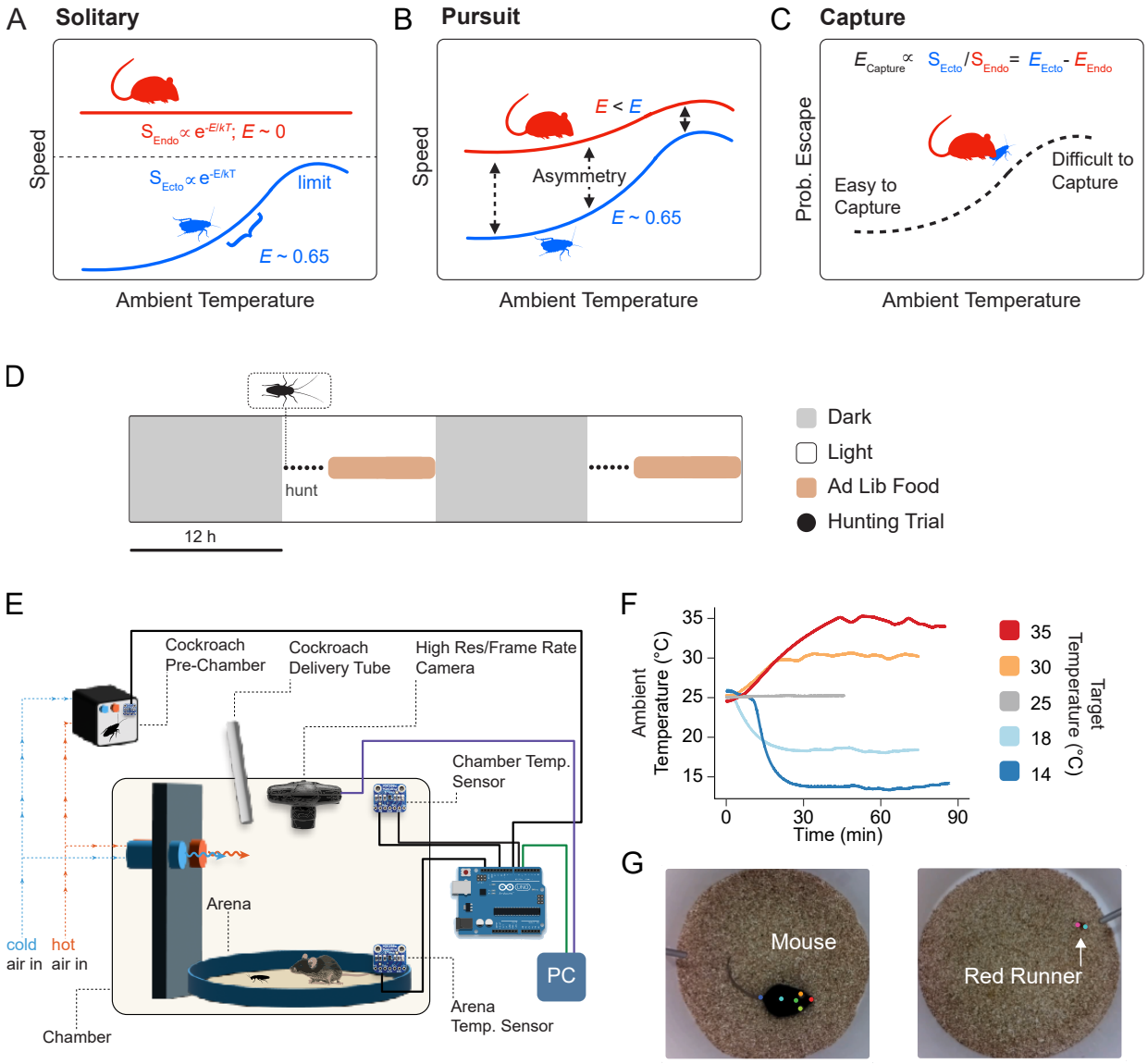

Figure 2: Schematic of endotherm and ectotherm locomotion and foraging. **(A)** In isolation, endothermic physiology and locomotion should be relatively stable across normal ranges in ambient temperature, but ectothermic prey will show an ∼exponential increase until reaching a limit. The thermal response is quantified by E, measured along the upward portion of the curve. **(B)** During pursuit, apparent differences in speed will be reduced as predator tracks prey and converges on its speed. **(C)** Nonetheless, this performance asymmetry will favor endotherms in cold conditions, where ectotherms are slowest. The differences in endo- and ectotherm thermal sensitivity from (A) predicts foraging outcomes. (**D**) To test model predictions, mice were offered red runners daily after food deprivation, up to six trials per day. (**E-F**) Hunting arenas were heated and cooled, and animal movement was tracked (**G**) using markerless pose estimation.

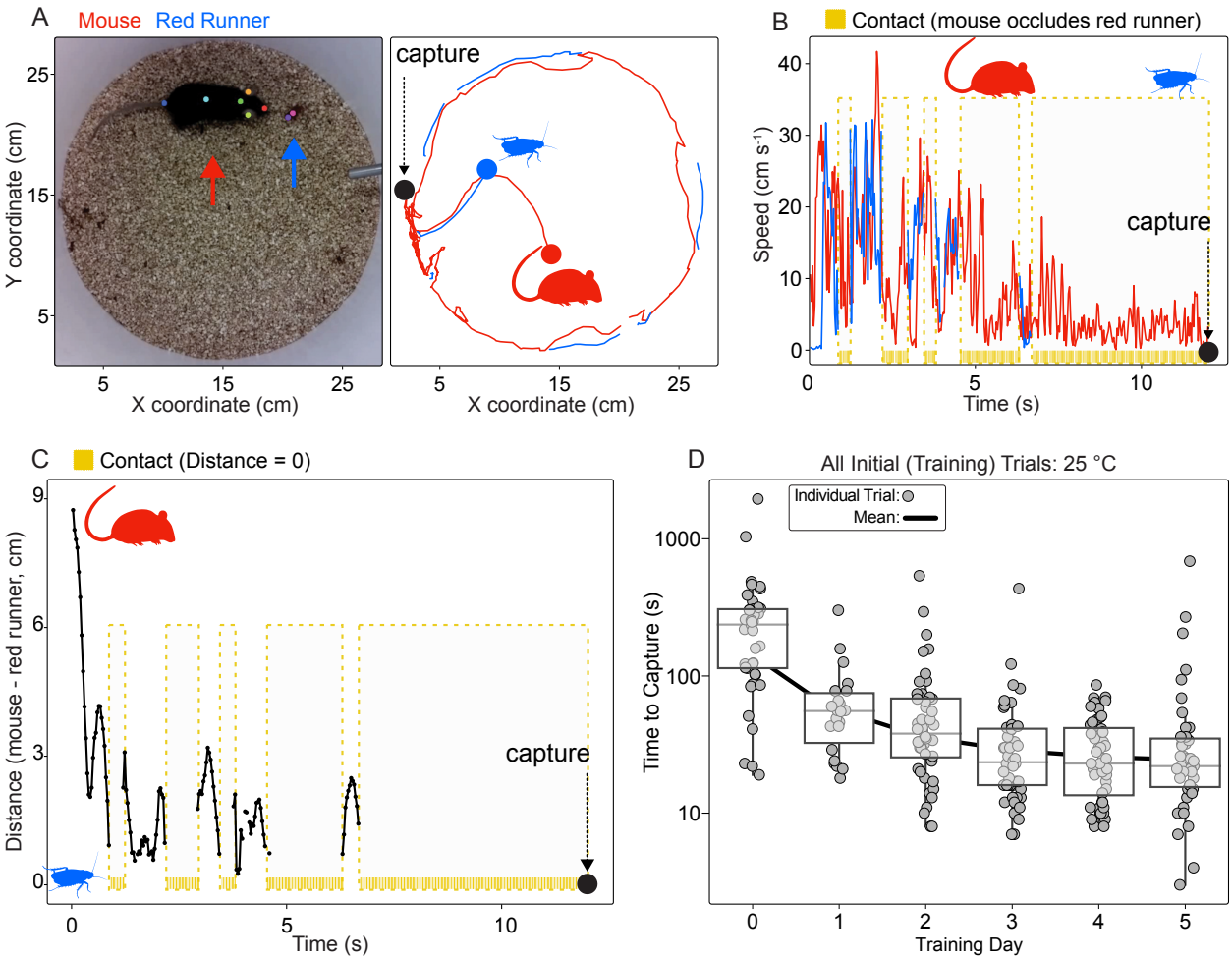

Figure 3: Laboratory mice rapidly learn to hunt and consume red runners. (A) (left) Video frame of mouse (red arrow) hunting a red runner (blue arrow). Colored points on the animals' bodies illustrate the pose estimation tracking of six points on the mouse and two points on the red runner; all points are tracked in each frame of video. Coordinates are used to reconstruct animal paths **(B)**, and components of foraging, such as locomotory rates **(C)**, distance between animals and contacts (where distance = 0), and the time to capture **(D)**. Mice approach asymptotic performance within three days of trials (N = 8 animals).

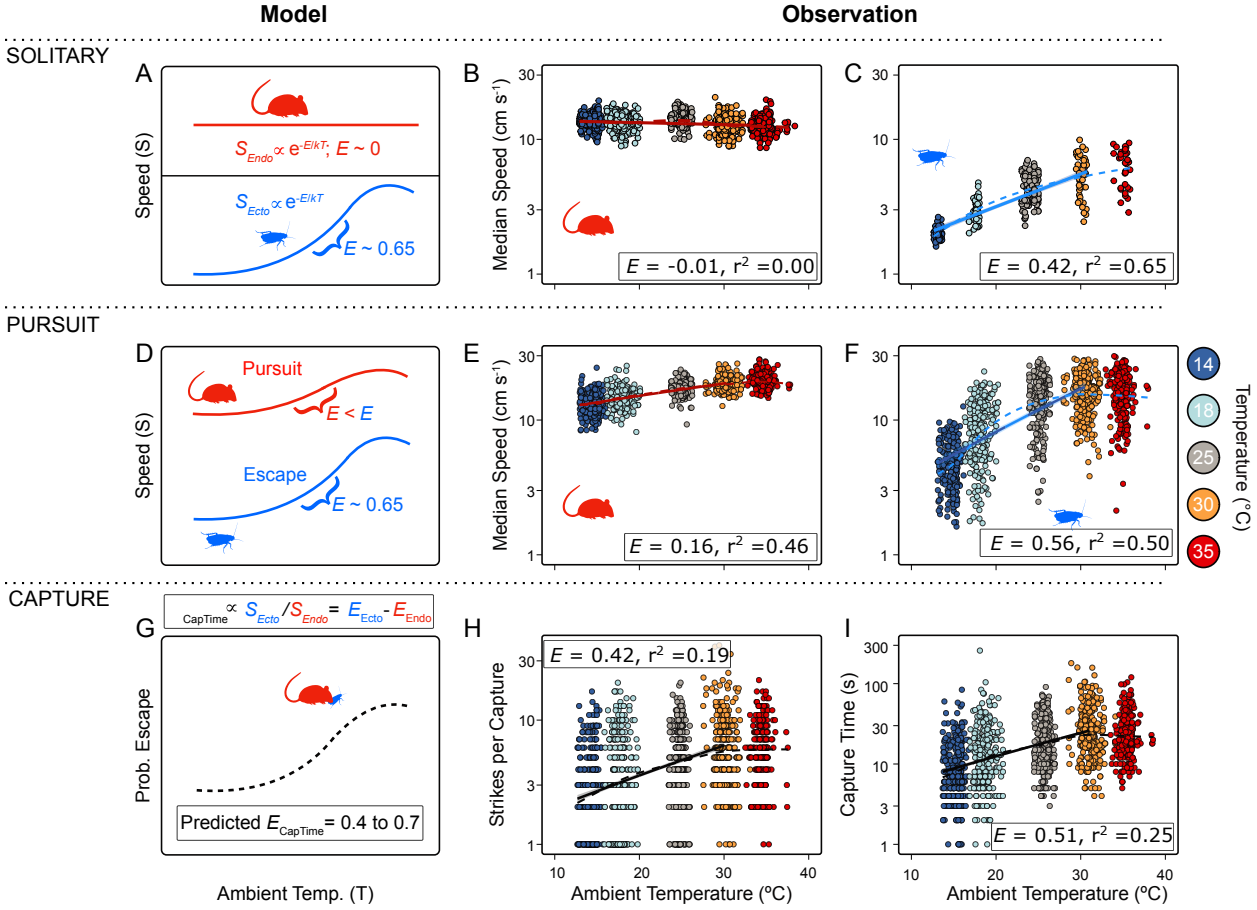

Figure 4: Endotherm hunting of ectotherms reflects metabolic asymmetries in performance. **(A)** In isolation, speed of endothermic mice should not depend on ambient temperature (T_a), where the thermal coefficient $E \sim 0$. In contrast, red runners are expected to increase speed with increasing temperature, $E \sim 0.65$. **(B-C)** As expected, median mouse speed is unaffected by temperature, while red runner median speed increases with temperature. **(D)** During pursuit, E_{mouse} is expected to be > 0 but $< E_{redrunner}$, since they modulate their speed to track prey; results are consistent with these predictions **(E-F)**. **(G)** The time to capture is predicted to reflect the difference in thermal sensitivity of maximum and median speed in mice and red runners in isolation (range: 0.43 – 0.67). Both the **(H)** strikes per capture and **(I)** capture times are near differences in E values from (B) and (C).

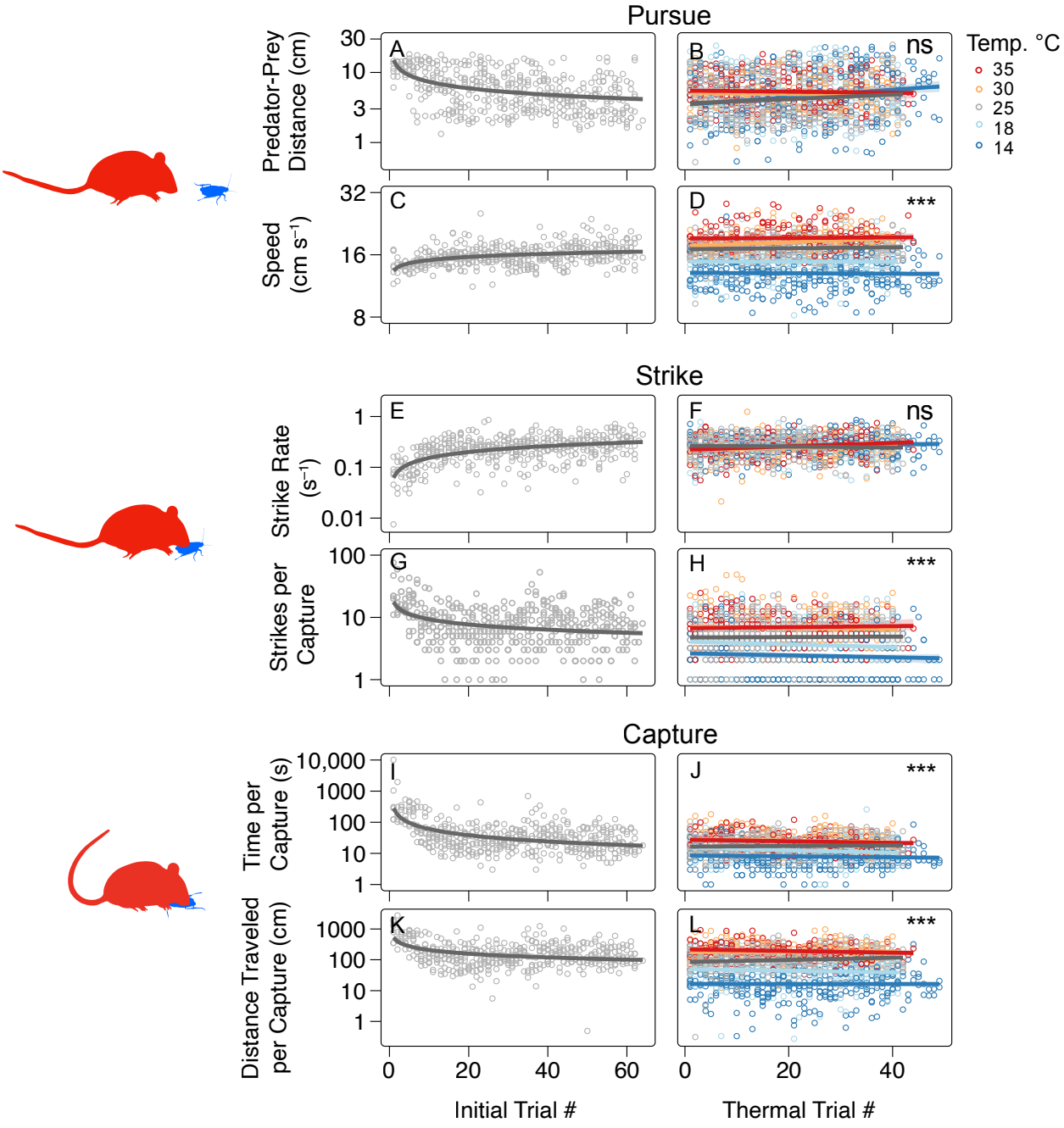

Figure 5: Temperature modulates most but not all features of learned hunting behavior. Left column: after initial exposure, mice improve performance over the course of initial trials, conducted at 25 °C. **(A, C)** As mice learn to pursue prey, they increase their speed and decrease the distance with prey. Strike rates increase with trial number **(E)** while strikes needed per capture declines over time as mice also become more efficient at hunting **(G)**. Over the course of initial trials, the time **(I)** and distance traveled **(K)** needed to capture prey declines. Right column: thermal trials following the initial trial period. **(B, D)** The average distance between predator prey is maintained across temperature regimes, as mice adjust their speed to match prey moving faster at warmer temperatures. **(F, H)** Strike rate is also invariant with temperature, though warmer temperatures require more strikes to subdue prey. **(J, L)** Ultimately, a strong thermal signal is observed for the time and distance traveled to capture prey. For left column, log response is regressed against log trial number.

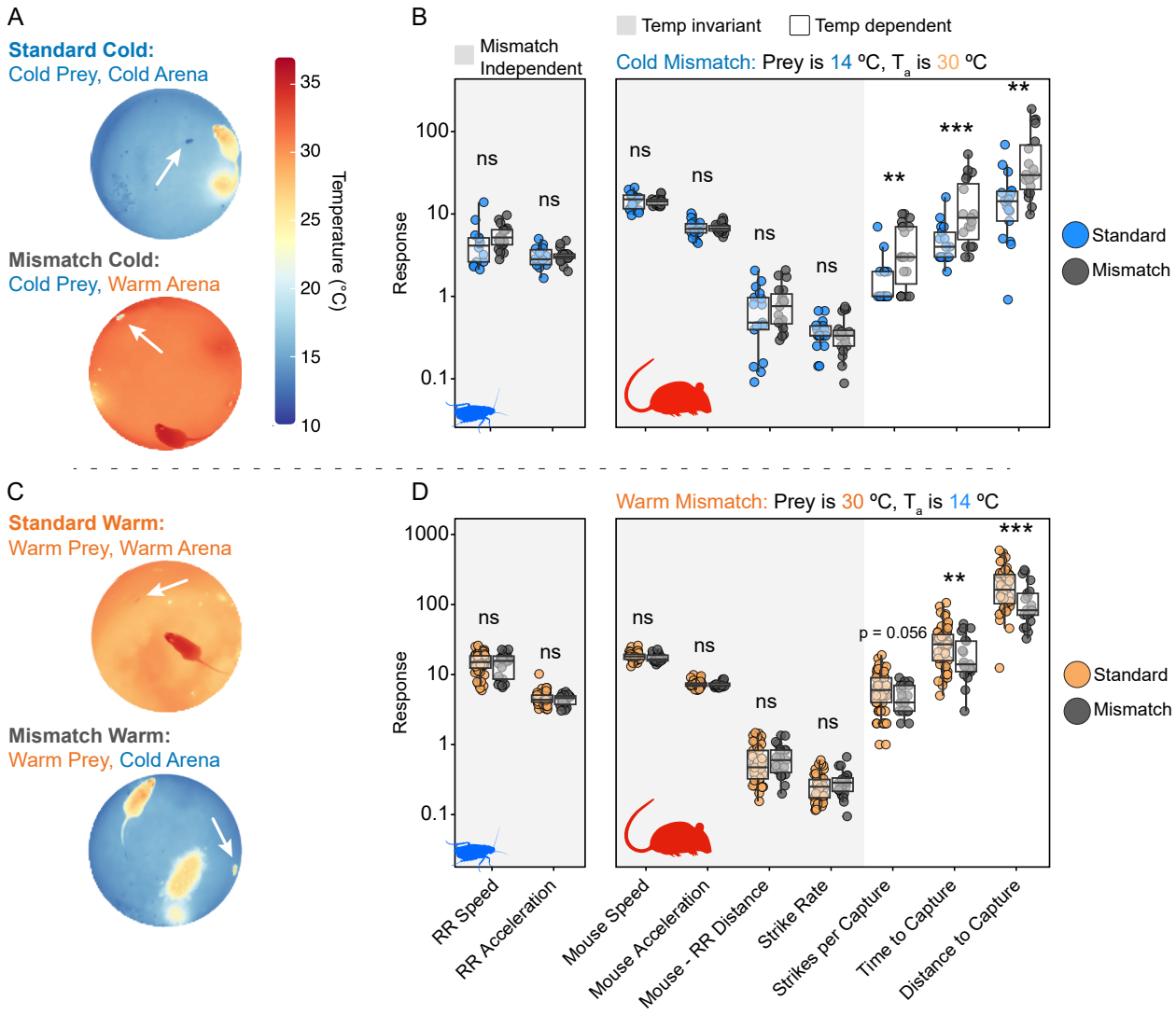

Figure 6: Mice use ambient temperature to guide hunting strategy. (A) Thermal image of hunting trials of a standard cold trial in which ambient temperature (T_a) and red runner body temperature (T_b) are both cold (Top). (Bottom) mismatch cold trial in which T_a is warm while red runner T_b is cold. White arrow indicates location of red runner. **(B)** Comparison of behavioral features as a function of condition: standard cold vs mismatch cold. Gray background indicates features expected to be invariant. White background indicates features expected to be temperature dependent. **(C)** Same as A but for standard warm and mismatch warm trials. (Top) standard warm trial in which ambient temperature (T_a) and red runner body temperature (T_b) are both warm. (Bottom) mismatch warm trial in which T_a is cold while red runner T_b is warm. **(D)** Same as B but for standard warm and mismatch warm. ns - not significant. $^{*}p < 0.05, ^{**}p < 0.01, ^{***}p < 0.001$. Effect sizes associated with significant values are $\geq |0.77|$.

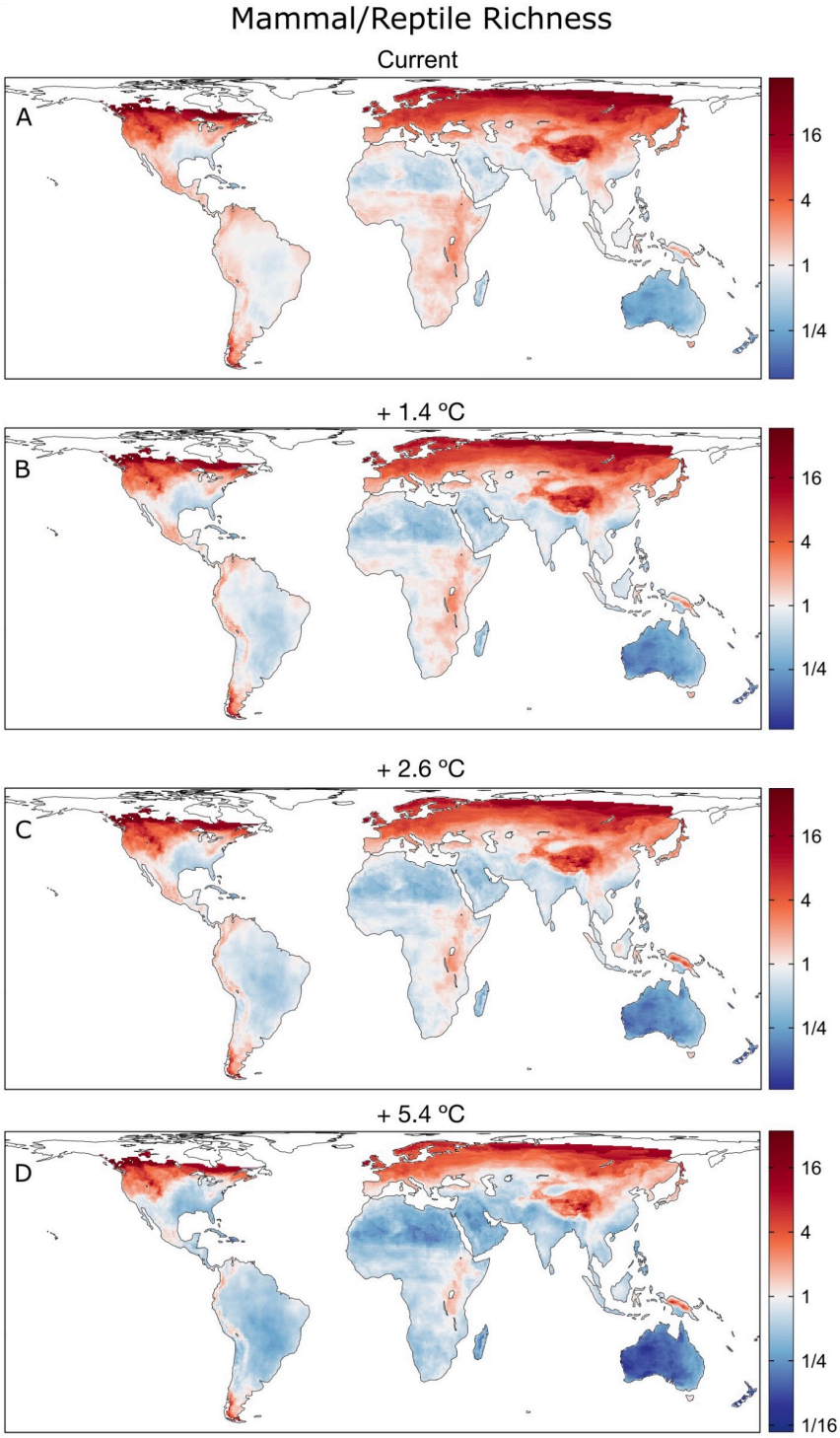

Figure 7: The ratio of mammal richness to reptile richness under three warming scenarios. For all plots, red colors indicates more mammals than reptiles, blue more reptiles than mammals, white is equal. **(A)**. Today, nearly 2/3 of the land's surface area has more mammals than reptiles. **(B-D)** Under multiple warming scenarios, the ratio of mammals to reptiles declines. Under the warmest scenario (D), today's pattern is inverted, with reptiles more diverse in 62% of the land's surface area.

Table 1: Thermal sensitivities (E) of hunting behavior. E is the thermal sensitivity, and locomotory rates are predicted to be 0.65 for ectothermic prey. During pursuit, endothermic mice are predicted to have nonzero thermal sensitivities lower than observed for prey. CI are confidence intervals, r^2 main is associated with the main effects, r^2 is for the full model where mouse id is a random effect. — indicates not applicable.

Thermal Rates	$E_{Predicted}$	$E_{Observed}$	CI	r^2 Main	r^2 Full
In Isolation					
Speed (Median)					
Red Runner	0.65	0.42	0.38, 0.46	0.65	—
Mouse	0	-0.0086	-0.017, -0.00014	0.0031	0.14
Speed (Maximum)					
Red Runner	0.65	0.64	0.59, 0.70	0.75	—
Mouse	0	-0.030	-0.048, -0.011	0.0082	0.098
Acceleration (Median)					
Red Runner	0.65	0.14	0.13, 0.15	0.68	—
Mouse	0	-0.00048	-0.0072, 0.0063	0.00	-0.13
Acceleration (Maximum)					
Red Runner	0.65	0.33	0.30, 0.36	0.68	—
Mouse	0	-0.014	-0.031, 0.0026	0.00	0.17
In Pursuit					
Speed (Median)					
Red Runner	0.65	0.56	0.53, 0.60	0.50	0.52
Mouse	< 0.56	0.16	0.15, 0.17	0.46	0.47
Speed (Maximum)					
Red Runner	0.65	0.62	0.60, 0.65	0.65	0.68
Mouse	< 0.62	0.27	0.25, 0.29	0.37	0.45
Acceleration (Median)					
Red Runner	0.65	0.19	0.17, 0.21	0.30	0.33
Mouse	< 0.19	0.074	0.066, 0.082	0.21	0.26
Acceleration (Maximum)					
Red Runner	0.65	0.42	0.40, 0.45	0.51	0.53
Mouse	0.42	0.25	0.23, 0.26	0.38	0.41
Mouse-Red Runner Distance	—	0.0036	-0.049, 0.056	0.015	0.11
Strike					
Strikes per Capture	—	0.42	0.38, 0.47	0.19	0.46
Strike Rate	—	-0.040	-0.0075, -0.0048	0.011	0.044
Capture					
Time per Capture	0.4-0.7	0.51	0.47, 0.55	0.25	0.56
Dist. per Capture					
Red Runner	—	1.4	1.3, 1.5	0.47	0.62
Mouse	—	1.1	1.0, 1.1	0.46	0.62

Supplemental Figures

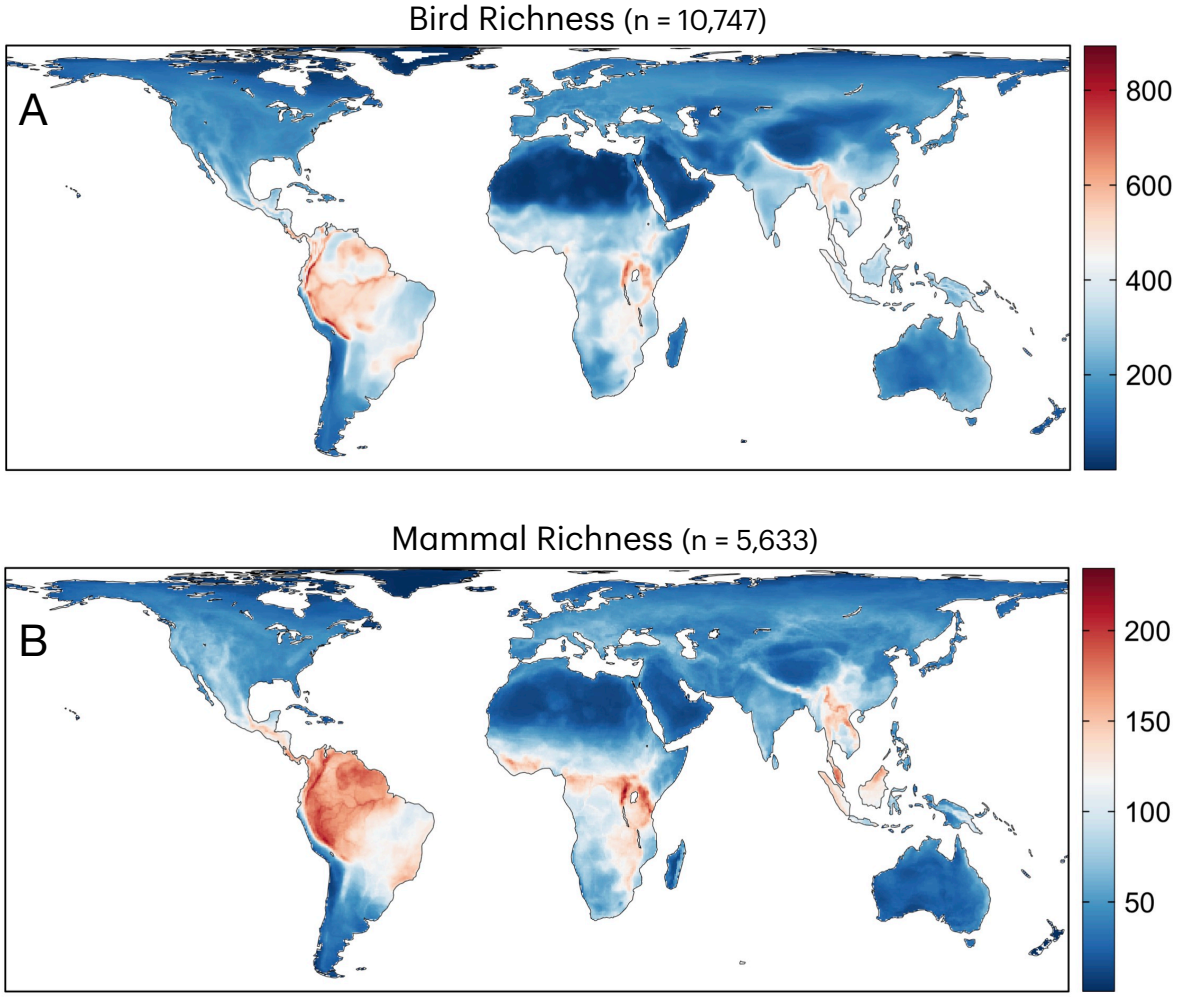

Figure S1: Global endotherm richness for birds and mammals. Richness was calculated by overlaying distributional maps and summing occurrence in a grid 48.25 km x 48.25 km.

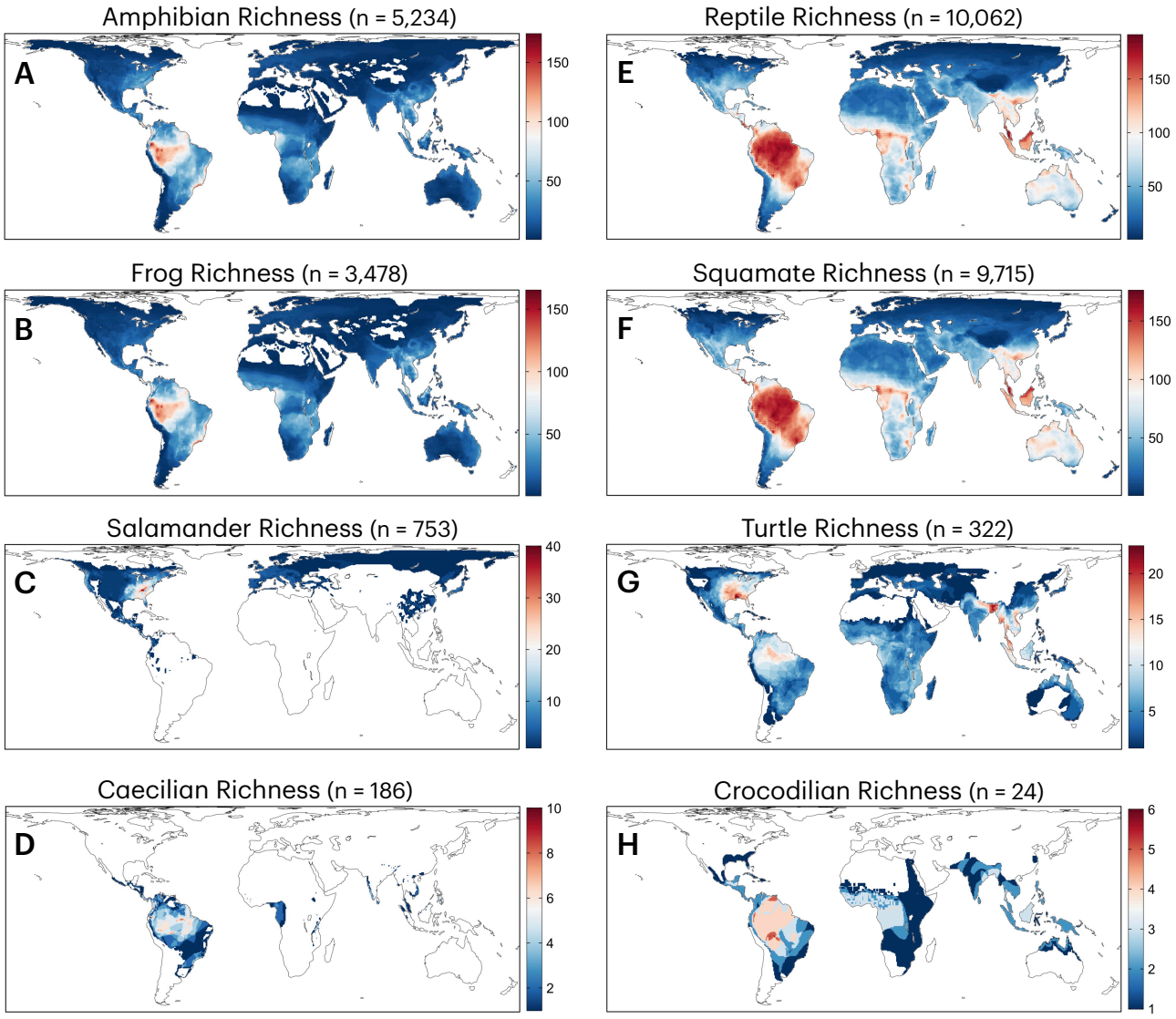

Figure S2: Global ectotherm richness. Richness for amphibian clades **(A-D)** and reptiles **(E-H)**. Grain size is 48.25 km x 48.25 km.

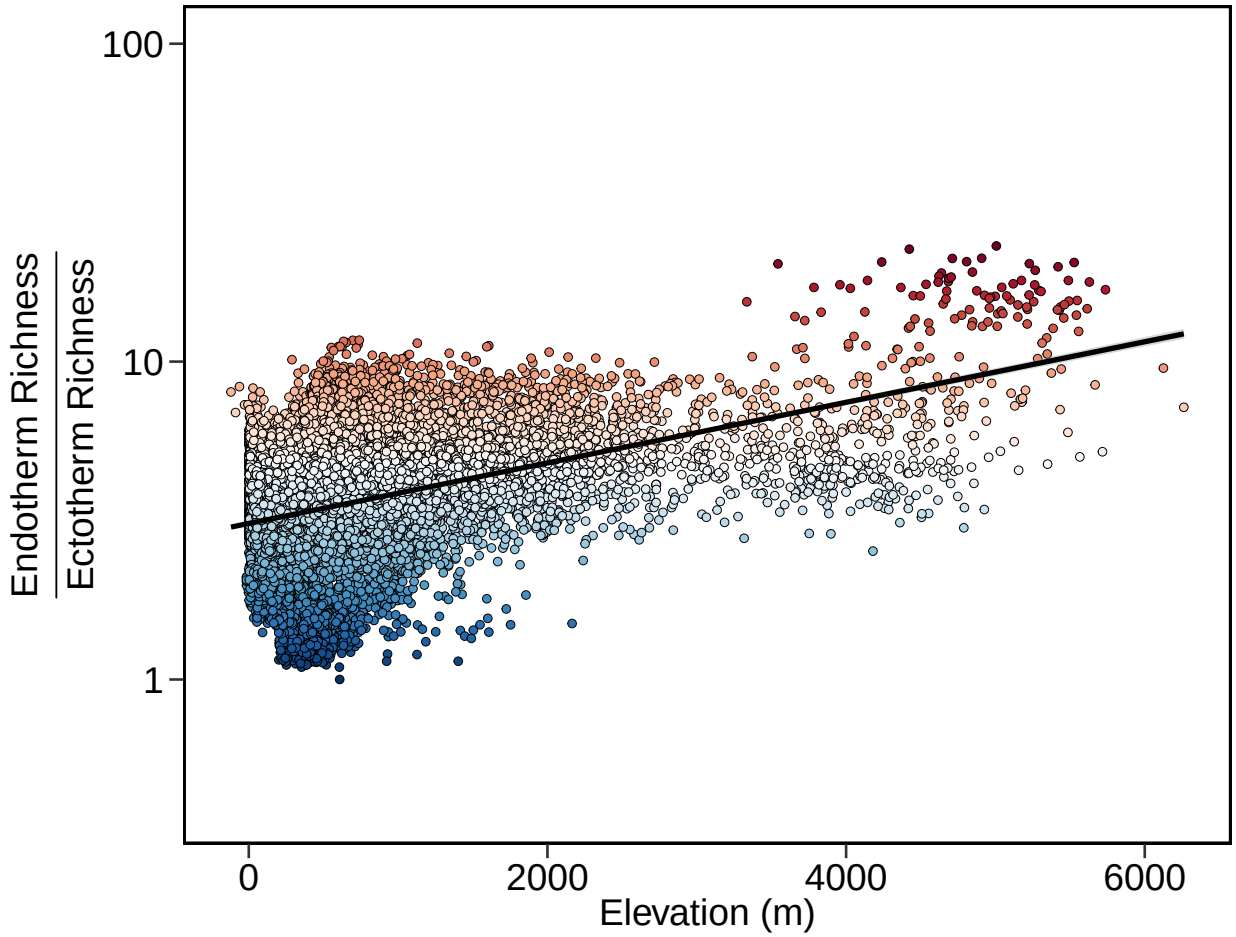

Figure S3: Vertebrate richness across elevation. The ratio of endotherms and ectotherm vertebrates over elevation. To control for thermal variation, data are restricted to tropical and subtropical latitudes, from -35°to 35°. y = 1.0 + 0.0030x, $r^2 = 0.27$, p < 0.001.

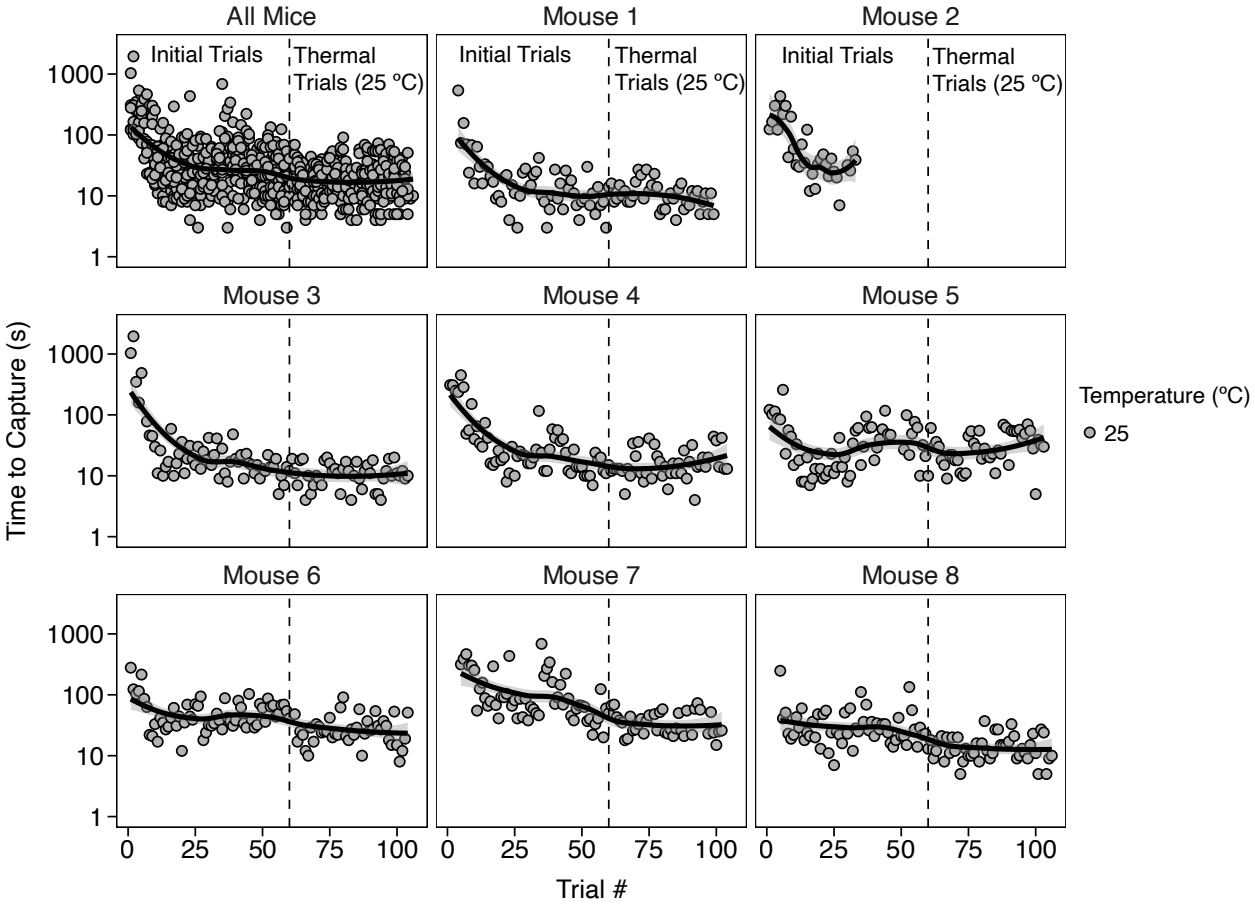

Figure S4: Individual Mice Learning Curves. Time to capture red runner prey declines with learning. For mice, the time to capture approaches an asymptote by the end of initial trials (dashed line), conducted at 25 °C. Subsequent thermal trials, including at the same temperature (right of dashed line), show only modest improvement, if any. LOESS fits from ggplot2.

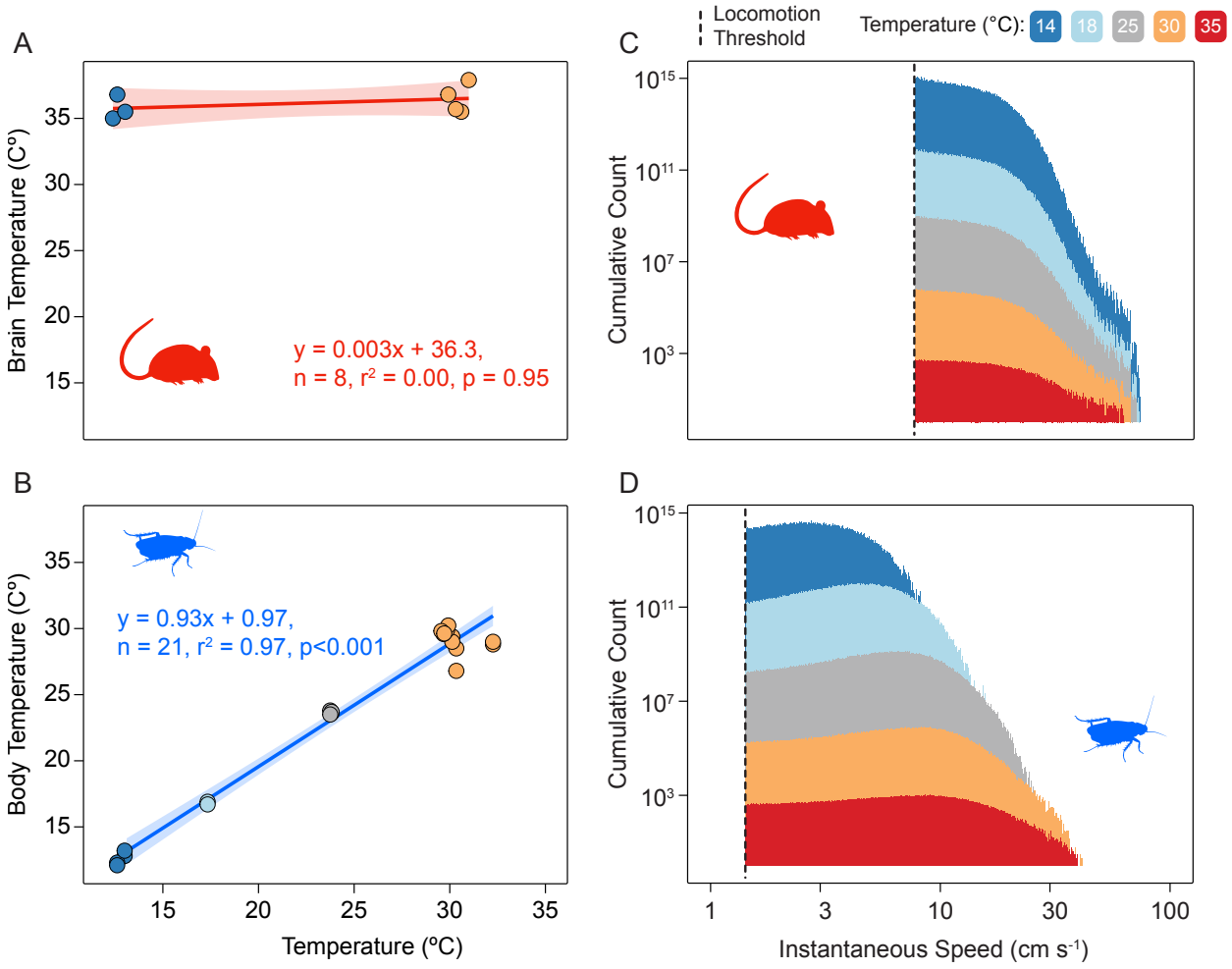

Figure S5: Thermal sensitivity of mice and red runners in isolation. (A) The internal temperature (brain temp: T_{brain}) of mice does not vary as a function of ambient temperature (T_a) between 14 and 30 °C). Mouse T_{brain} was measured by neuronal temperature probe in 8 animals (4 per temperature). **(B)** In contrast, red runner body temperature (T_b) is almost identical to ambient, with a slope near 1. T_b was measured by thoracic temperature probe in a total of 21 red runners across four temperatures between 14 and 30 °C. **(C)** Cumulative, stacked histogram of frame-to-frame speeds of mice in isolation at five temperatures between 14 and 35 °C, where each frame is 1/30 s. The threshold for locomotion (vertical dashed line) represents the empirically determined velocity threshold that reliably separates locomotion from other movements. Note mouse distributions of movement in isolation are similar at every temperature. **(D)** In red runners, the threshold for locomotion is lower than mice due to the absence of measurable postural adjustments at rest (See Fig. S7 for thresholds). Note the increasing shift in median and maximum speeds of red runners with temperature.

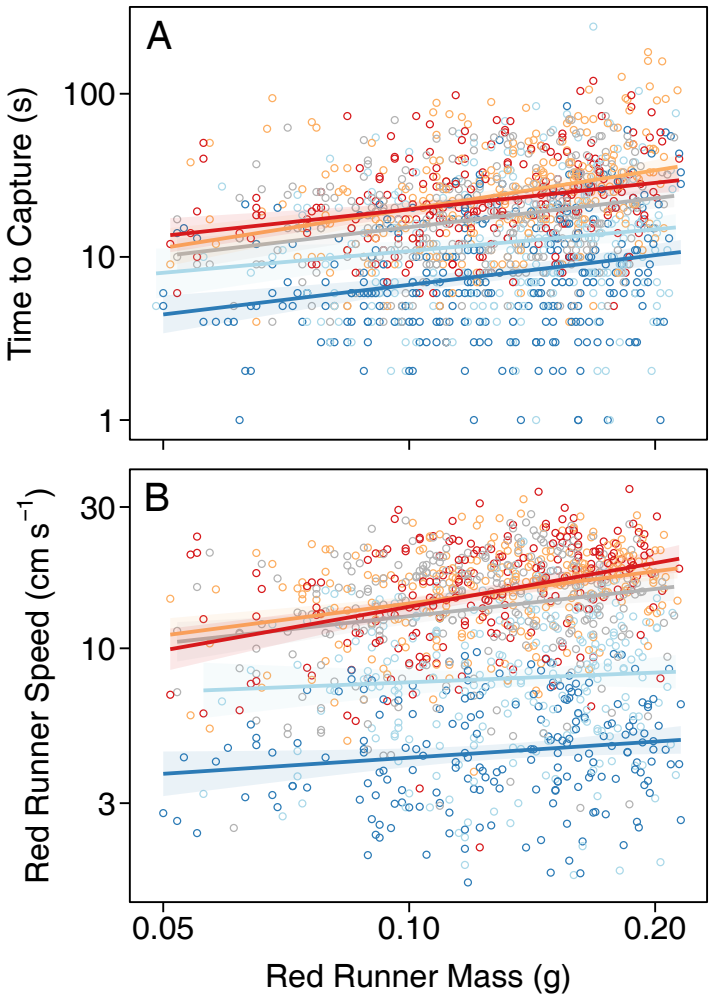

Figure S6: The effects of red runner mass on speed and time to capture. As red runner mass increases, the time to capture increases **(A)**, and red runner speed increases **(B)**. Color indicates thermal trial temperature, from 14 °C (blue) to 35 °C (red).

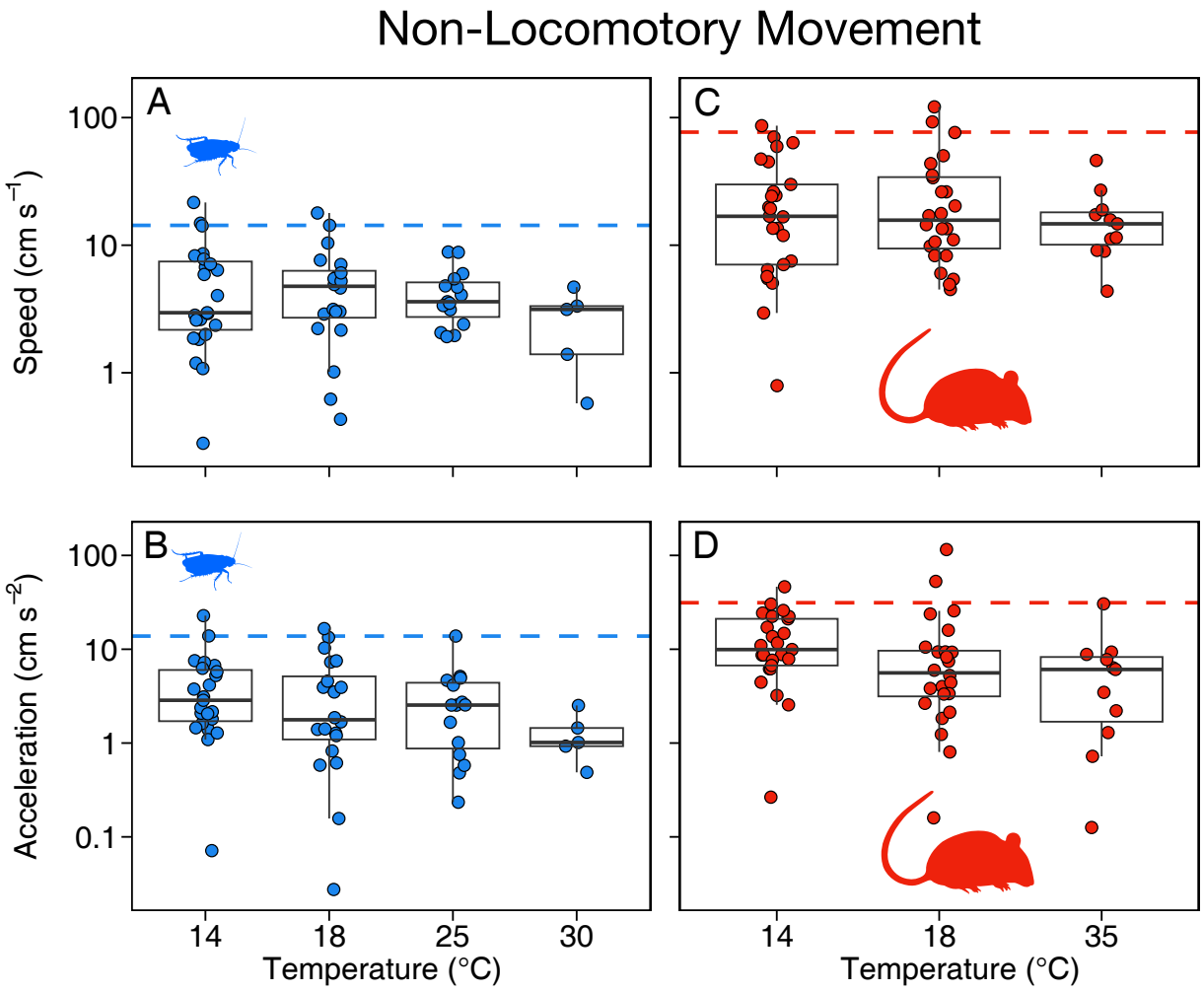

Figure S7: Non-locomotory movement. Videos were manually reviewed and frames noted when animals were not locomoting but movement was detected. This can reflecting non-locomotor movement like grooming, or video artifacts from pixel jittering. 95% quantiles are indicated by the dashed lines, and these were used as a threshold to distinguish locomotory from non-locomotory motion. Red runners **(A, B)** have lower thresholds than mice **(C, D)**, which exhibit more postural movements during grooming.

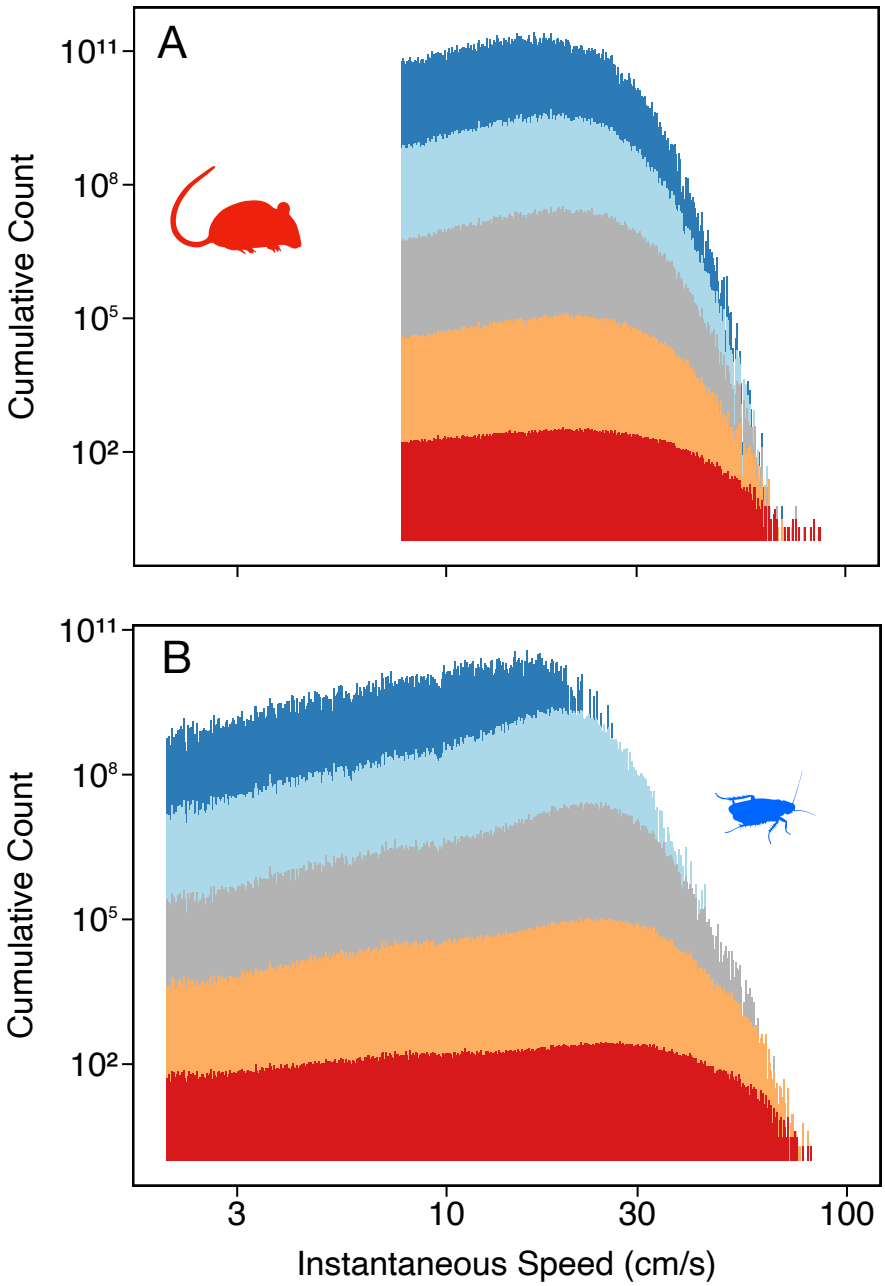

Figure S8: Thermal sensitivity of mice and red runners speed during a hunt. (A). Mouse and **(B)** red runner frame-frame speed during a hunt, where each frame is 1/30 s. There is a stronger signal of temperature for red runners during a hunt. Note for (A-B), the lower speeds are truncated below a threshold where non-locomotory movement is observed (See Fig. S7).

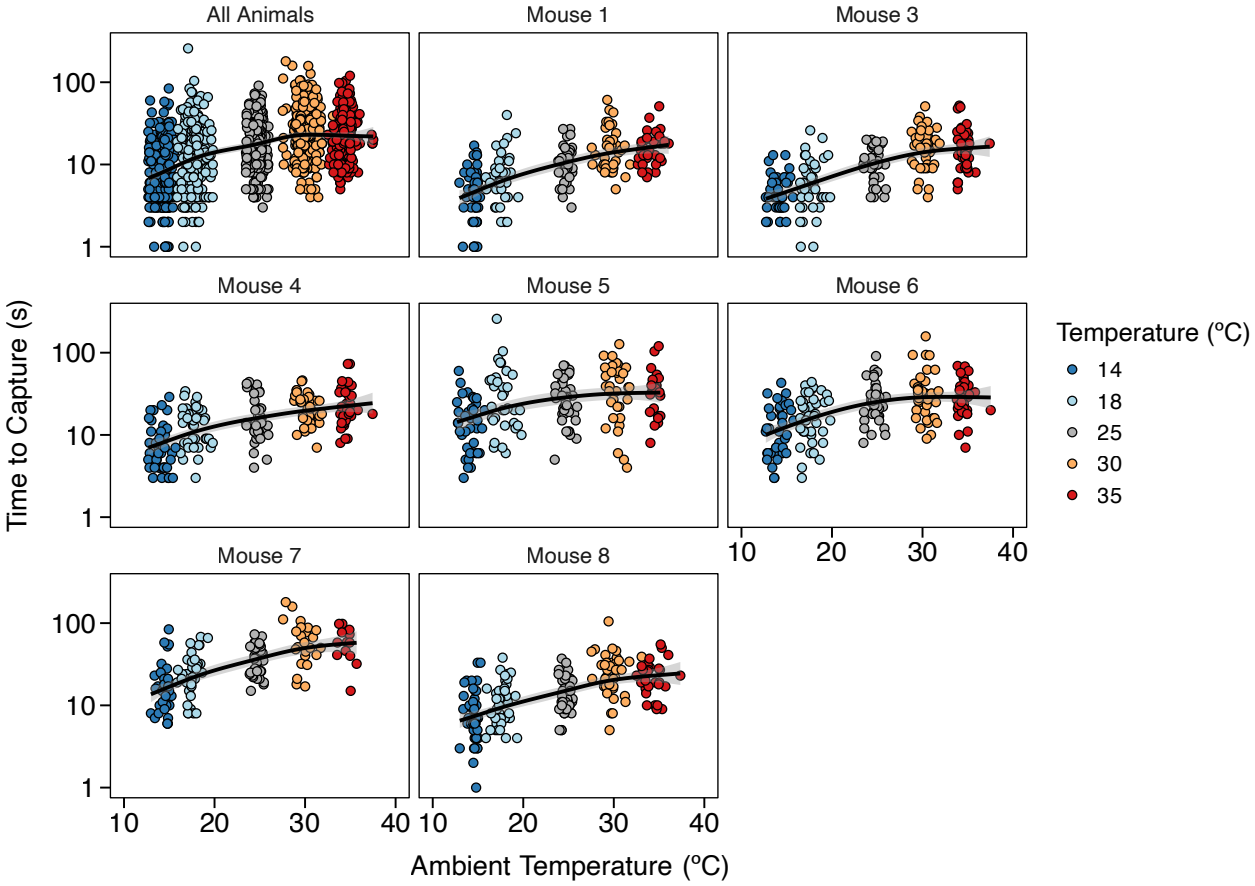

Figure S9: Individual Mice Thermal Hunting Results. When pooled, all animal show a strong thermal effect of temperature with respect to temperature, but similar patterns are observed when considering animals separately.

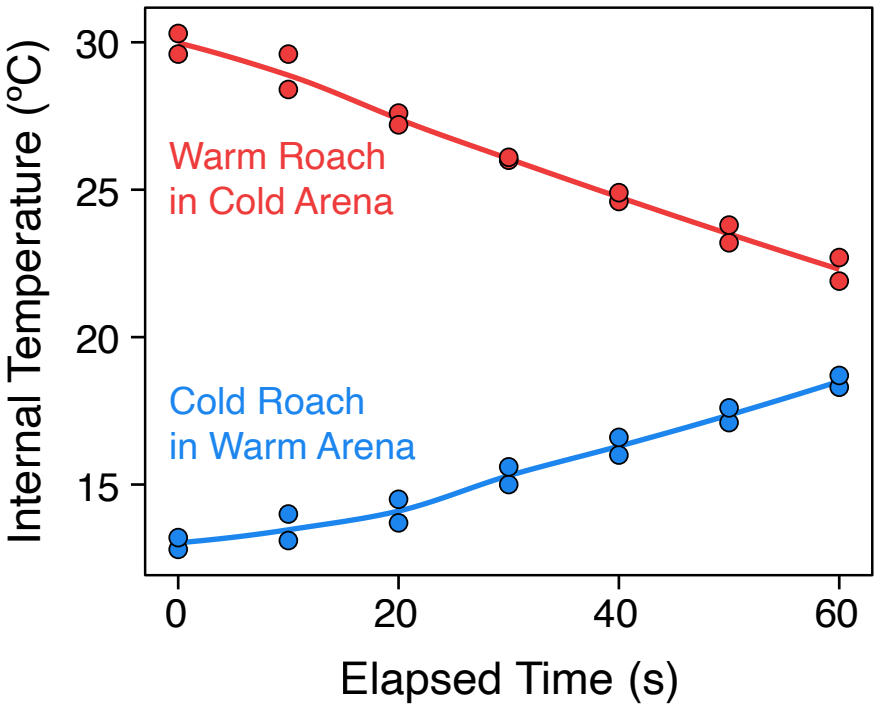

Figure S10: Internal body temperature of red runners at warm and cold conditions. For mismatch trials, body temperature match ambient temperatures initially, but warm roaches eventually cool in cool arenas and vice versa. Note, however, that the time to warm or cool more than a few degrees is well after the typical time to capture, ∼5-15 seconds.

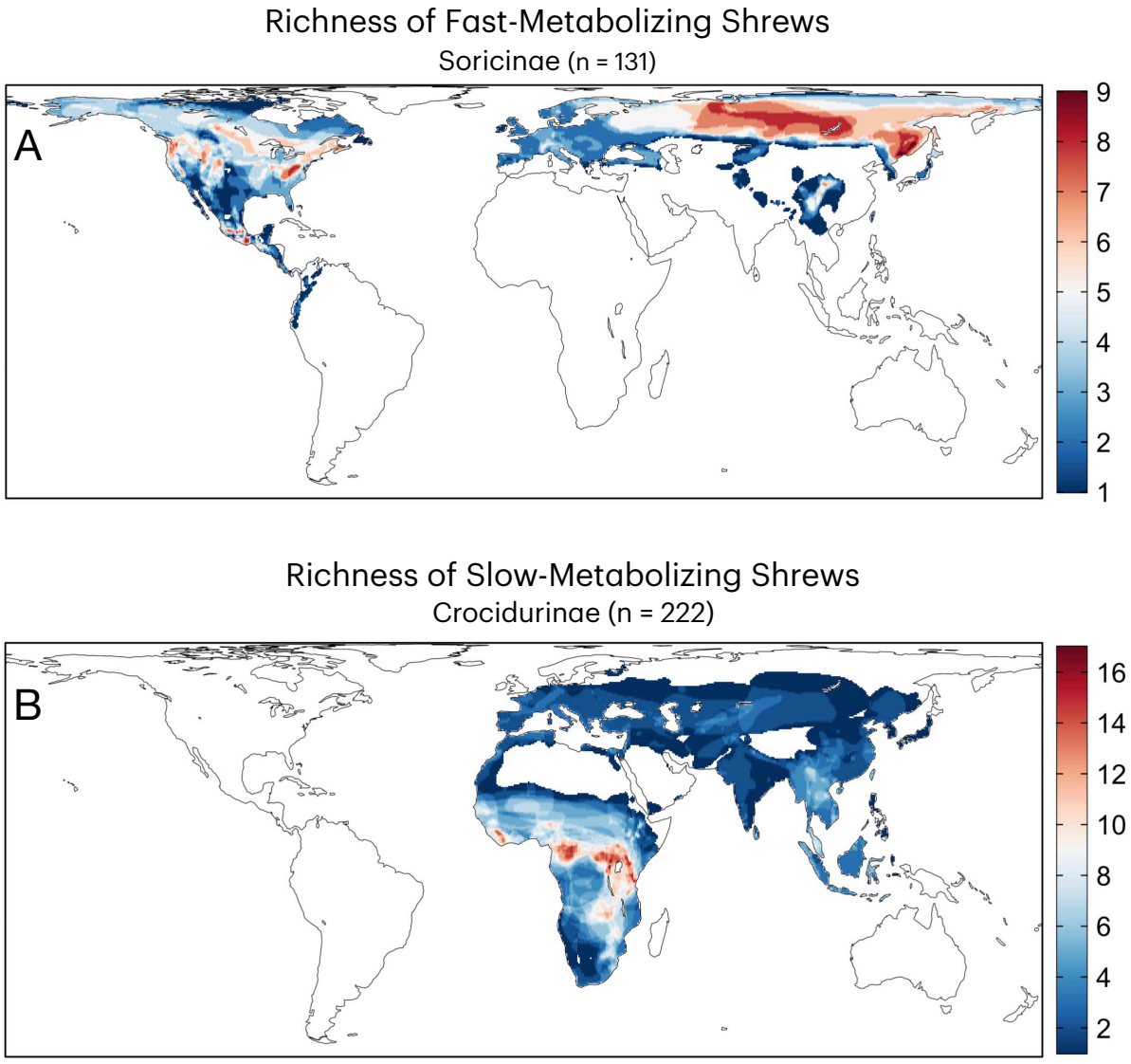

Figure S11: Global shrew richness. Richness for **(A)** fast-metabolizing red-toothed shrews (subfamily Soricinae) and **(B)** white toothed shrews (subfamily Crocidurinae). Note the temperate peaks in diversity for Soricinae. White toothed shrews have approximately half the metabolic rate as red-toothed shrews and have a more typical tropical peak in diversity (B).

Table S1: Slopes for linear and spatial models of vertebrate richness. *E* coefficients for a Bayesian linear model and the spatial Bayesian hierarchical model: Besag-York-Mollié 2 (BYM2). 95% credible intervals and deviance information criterion values are provided.

Table S2: Means and associated p values and Cohen's D effects sizes are provided for mismatch trials. Abbreviations: acc is acceleration (cm s^{-2}), q50 is median, vel is velocity (cm s^{-1}), strikes_n is the number of strikes per trial, time_s is the time required per capture (s), dist_travel is the distance traveled per hunting trial (cm), snout_roach_dist is the distance between mouse and red runner (cm). 'Cold' refers to trials at 14 °C, 'warm' are trials at 30 °C.

Methods

Terrestrial Vertebrate Distributions and Diversity

Species distributions for vertebrates were acquired from publicly available datasets. Mammal and amphibian distributions were from obtained from the IUCN[44], bird distributions from BirdLife International[45], and reptile diversity from Roll et al. (2017)[46]. To calculate species richness, we used the Behrmann equal area projection with a WGS84 grid of 48.25 km x 48.25 km, corresponding to ~ 0.5˚x 0.5˚at 30˚latitude. An occurrence was recorded wherever species distributions overlapped any part of the grid. These occurrences were then summed to calculate richness.

Global analyses of vertebrate diversity tend to focus on a few independent drivers: temperature, elevation, and precipitation[2]. To calculate the change in richness with temperature we used the following formulation log(endo_rich/ecto_rich) = (1/kT) + log(precipitation) + elevation_range. Substitution of elevational standard deviation for range did not change results. Of these three drivers, temperature was the most important factor by far: *partial* r^2 temperature: 0.79, precipitation: 0.092, and elevation: 0.011 (package rsq[47]). We accounted for spatial autocorrelation in our analysis using the Besag-York-Mollie 2 (BYM2) model[48], implemented in R-INLA[49]. BYM2 is a spatial Hierarchical Bayesian model that partitions random effects into spatially structured and unstructured components, and uses penalized complexity priors to avoid overfitting. R-INLA employs efficient integrated nested Laplace approximations of posterior distributions. See Table S1 for spatial results.

Climate Projections

Temperature forecasts were from IPCC 6 projections (Intergovernmental Panel on Climate Change), based on specific climate change scenarios known as Shared Socioeconomic Pathway (SSP), using the Coupled Model Intercomparison Project Phase 6 (CMIP6) data[26,27]. Data were taken from CESM2 model of CMIP6 climate projections. Specifically, we used SSP 1-2.6 to project a global average of 1.4 °C by 2100 (low emission pathway)[28], SSP 2-4.5 to project an average 2.6 °C increase ("middle of the road")[29], and SSP 5-8.5 for the 5.4 °C increase (high emissions)[30]. Suffixes correspond to the increase in watts per squared meter between 1750 and 2100 from carbon emissions; e.g., SSP5-8.5 assumes an increase of 8.5 W/m^2. Data were downloaded from https://cds.climate.copernicus.eu, and standardized to 48.25 km x 48.25 km Behrmann equal area projections.

To forecast changes in comparative richness (Fig. 7), we first calculated the deviation in near surface temperature and precipitation from today vs climate model projections. Next, to generate spatially explicit projected deviation in richness, we multiplied this deviation by the coefficients from the linear mixed model fit: lm(log(endo_rich/ecto_rich) $\sim$ (temperature_C) + log(precipitation) + elevation_range). Finally, we added the projected deviation to current endo_ecto richness to generate future estimates of comparative diversity.

Metabolic Asymmetry Theory

Metabolic and locomotory rates generally increase with temperature until reaching a peak, and then decline until they cease with death. The thermal dependence of metabolic and performance rates in the upward portion can be written as:

$$Rates \propto e^{-E/kT} \tag{3}$$

where k is Boltzmann's constant, T is temperature in Kelvins and E is a thermal sensitivity coefficient ('activation energy'), which is ~ 0.65 for metabolic rate[9] and was found to be ~ 0.5

for locomotion by Dell et al. (2011)[25]. Red runner performance increased until 30 °C in our experiments. Therefore, we only consider estimates of E up to 30 °C; similarly, for comparison, we report only estimates of E in mice up 30 °C.

Previously, we published a theoretical model to explain elevated endotherm diversity at high latitudes in the ocean[14]. We argued that the asymmetric metabolic and performance response to ambient temperature between endotherms and ectotherms implied higher performance rates and ecological success of endotherms in the cold, as ectotherm prey, predators and competitors become cold and sluggish.

A key prediction of this Metabolic Asymmetry Theory (MAT) is that the probability of capture $P(Capture)$ after detection is a function of the difference in thermal sensitivity between endotherms and ectotherms during a predation event. Specifically, $P(Capture) \propto \Delta E^{\alpha}$, where ΔE is the difference in thermal sensitivity of locomotion between predator and prey, and $\alpha < 1$. Note for an endothermic predator and ectothermic prey, α may be less 1 if predators use learned or cooperative behaviors to reduce the kinetic difficulties of capturing fast-moving ectotherms, such as dolphins herding prey. In addition, where predator speed $\gg$ prey speed, $\alpha \to 0$. For instance, for endotherms foraging on immobile or slow moving prey (e.g., plants or snails), changes in temperature will not affect the probability of capture. In our experiments, red runners required pursuit and were relatively challenging to catch, at least at warmer temperature. Additionally, mice were not expected to have special strategies for dealing with faster prey, so in our experiments we expect $\alpha = 1$, and ΔE^{α} simplified to ΔE.

Because prey are in a confined area, $P(Capture) = 1$ as long as predators are motivated. Thus we used time to capture as a proxy for probability of capture. Longer times to capture correspond to lower probability of capture in nature or, equivalently, a higher probability of escape.

To define ΔE, we considered differences in the thermal sensitivity of speed rather than acceleration because capture involved unobstructed pursuit around the contours of the arena; for ambush predators, acceleration may be more relevant in cases of ambush. In isolation, the difference in thermal sensitivity of median speed (ΔE_{Speed}) = 0.43; for maximum speed, ΔE_{Speed} = 0.67. We use both these median and maximum values to establish a range for ΔE_{Speed} (0.43 − 0.67) predicted to determine the thermal sensitivity of time to capture ($E_{CaptureTime}$).

Experimental Methods

Experimental model and subject details: All experimental procedures were conducted in accordance with protocols approved by the Washington University in Saint Louis Institutional Animal Care and Use Committee (IACUC), following NIH guidelines for the care and use of research animals. Five female and three male C57BL/6J mice (Supplier: The Jackson Laboratory) were used in this study. Mice were seventeen weeks old at the time of prey capture experiments. We observed no differences in predation between male and female mice and, therefore, combined their data. Turkestan red runner cockroaches (Supplier: Caribbean Mealworms) aged three to four months and weighing 0.05 - 0.20 g (mean = 0.1 g), were used as prey for all capture experiments.

Prey capture experiments: Forty-eight hours prior to the commencement of hunting trials, mice were housed individually in circular hunting arenas (36.83 cm H x 25.87 cm D) and provided with food pellets and water ad libitum. The arenas, which also served as home cages for the duration of the experiments, were located in ventilated and temperature-controlled chambers on a 12:12 light/dark cycle (Fig. 2E-G). After forty-eight hours of the mice habituating to these new enclosures, three red runners were introduced to each room temperature (i.e., 25 °C arena overnight

(i.e., 12 h dark period), alongside ad libitum access to food pellets. Any red runners that remained at the end of the 12 h dark period were then removed. This protocol was repeated for 1 d for a total of 2 d of pre-exposure to red runners in dark conditions.

Ten days of hunting trials were then conducted at room temperature. Food pellets were removed 14 - 16 h before each day of hunting trials, which commenced 1 h after the onset of the light period. After the conclusion of each day of hunting trials, food pellets were returned to the arenas for 8 - 10 h (Fig. 2D). Each trial consisted of a red runner being placed in the arena, and the interactions of mice and red runners were recorded with an overhead camera (30 fps; e3Vision; White Matter). Ten minutes following a successful capture, a new red runner was introduced. Each day, the mice had the opportunity to capture up to six red runners each ($\sim$ 60 trials total per mouse).

Thermal trials were conducted after 10 d of initial room temperature hunting trials. Thermal trials were carried out at the following temperatures: 14, 18, and 25 (room temperature), 30 and 35 °C (Fig. 2F). Each day of thermal trials was conducted as stated in the previous paragraph, with the addition of ambient temperature control. Specifically, for each day of thermal trials, the experimental chambers containing the red runners and mice were maintained at the target temperature across all trials, beginning 30 min prior to the commencement of the first trial. Thermal trials were conducted in two experimental phases: in the first phase, which was conducted for 27 d, the target temperature was switched every 5 d ($\sim$ 30 trials total per temperature per mouse). In the second phase, which was conducted for 10 d, the target temperature was switched every 1 d ($\sim$ 12 trials total per temperature per mouse). To control for thermal trial order effects, half of the mice experienced cold conditions before warm and half experienced warm conditions before cold.

Thermal mismatch trials were conducted after 37 d of thermal trials. In contrast to the thermal trials in which the red runners and mice were maintained at matching target temperatures, thermal mismatch trials involved maintaining red runners at a different temperature than the mouse arenas to which they were subsequently introduced. Specifically, cold red runners (cooled to 14 °C) were placed into warm mouse arenas (heated to 30 °C) and vice versa (Fig. 6A,C). Thermal mismatch experiments were conducted for 12 d total, with the direction of the mismatch switching after 6 d. Across each set of 6 d, standard (i.e., matched) thermal trials were carried out as previously described (i.e., 6 trials per mouse per day), except every other day in which a thermal mismatch trial was substituted for trial no. 1 and followed by five trials in matched conditions (3 mismatch trials total per mouse across each set of 6 d).

Movement tracking and analysis: Videos of mice and red runners were recorded with an overhead camera (30 fps; e3Vision; White Matter). Each trial was manually scored for time to capture and scoring accuracy was verified on a subset of videos by two trained scorers. Markerless pose estimation was conducted on the mouse and red runner using DeepLabCut[50] (Fig. 3A), specifically tracking six anatomical points on the mouse (snout, left ear, right ear, shoulder, spine, tail base) and two points on the red runner (front and back). Based on these six anatomical points, other points were extracted using midpoint calculation $\left(\frac{x_1+x_2}{2}, \frac{y_1+y_2}{2}\right)$, e.g., red runner center. After this, second-order features such as distance traveled ($\sqrt{(x_1-x_2)^2+(y_1-y_2)^2}$), velocity ($\left|\frac{d}{dt}\text{distance traveled}\right| \times \text{fps}$), and acceleration ($\left|\frac{d}{dt}\text{velocity}\right|$) were calculated for each animal (custom Python script). Strikes between mouse and red runner were defined as when both points on the red runner were occluded by the mouse for $\geq \frac{1}{3}$ s (Fig. 3C). Additionally, red runner movement was calculated with respect to red runner center while mouse movement was calculated with respect to mouse spine.

Video post-processing: Videos were recorded at 30 fps and markerless pose estimation was

conducted on the mouse and red runner using DeepLabCut[50] across 9 million total frames. Occasionally, the DeepLabCut model would produce erroneous pose estimate values, so a series of post-processing steps was conducted to identify and remove outliers (custom R script). First, for each video, a frequency distribution of the change in spatial position from one frame to the next was inspected for outliers and then compared to the corresponding video segment to determine a conservative threshold for exclusion. Specifically post estimate values were excluded if the distance traveled from one frame to the next exceeded 3 cm (equivalent to 90 cm/s). Additionally, red runner pose estimate values were discarded if the front and back values differed by more than 2 cm (i.e., exceeding body length).

Next, movement values were excluded that did not reflect locomotion. This was defined as the 95% quantile of speed and acceleration for mice or red runners that were visually confirmed to be stationary in videos (Fig. S7). This may reflect artifacts of the DeepLabCut pose estimate (e.g., pixel jittering) or true non-locomotory movement (e.g., like grooming).

Finally, we used the following outlier formula to identify and exclude the remaining outliers: $Q2CIQR$, where $Q2$ is the median, IQR is the $25-75\%$ inter-quartile range, and C is a coefficient. (Note that $C = 1.5$ is the outlier range in a traditional box plot, equivalent to 2.7 standard deviations in a normally distributed dataset). For a given trial, we used $C = 3$ (equivalent to 4.5 standard deviations), and for pooled red runners or mice at each temperature, we used $C = 6$ (equivalent to 9 standard deviations).

Mouse brain temperature recordings: Mice were placed in temperature-controlled chambers (14 °C, n = 4; 30 °C, n = 4) for 30 minutes and then rapidly anesthetized with 5% isoflurane. Upon confirmation of loss of consciousness ($\sim$ 10 s), each mouse was decapitated and then a sterile temperature probe was immediately inserted into the brainstem via the foramen magnum. Temperature data were collected for 5 s at a frequency of 1 Hz and were recorded with a digital dual channel thermometer (Leaton) (Fig. S5A).

Red runner internal temperature recordings: Red runners were placed in temperature-controlled chambers (14 °C, n = 4; 18 °C, n = 2; 25 °C, n = 4; 30 °C, n = 11) for 30 minutes and then a sterile temperature probe was inserted into the abdomen of each red runner. Temperature data were collected for 5 s at a frequency of 1 hz and were recorded with a digital dual channel thermometer (Leaton) (Fig. S5B).

Thermal imaging: Naive mice and red runners were placed in temperature-controlled chambers that were either cooled or heated to 14 °C or 30 °C, respectively. After 30 minutes, one mouse and one red runner from matched thermal conditions (i.e., 14 °C and 30 °C) were paired together and imaged using a thermal camera (FLIR E53; Teledyne FLIR). This imaging protocol was repeated with mice and red runners from mismatched thermal conditions (Fig. 6A,C).

Statistical Analysis of Experiments

All analyses were performed in R, using packages 'tidyverse' for data manipulation and plotting, and 'lme4', 'lmerTest', and 'emmeans' for mixed model analysis. Nonlinear fits in Fig. 3and Fig. S4 are LOESS fits generated in 'ggplot2'. See code for full details.

A linear mixed model was fit to log transformed response rates to estimate the value of parameter E, using the R packages 'lme4' and 'lmerTest'. In chemical kinetics, E serves as a theoretical measure of thermal sensitivity, with an average value of $\sim$ 0.65 electron volts (eV) for metabolic rate studies, where $log(rate)$ is proportional to $exp(–E/kT)$. Note, $E = \sim$0.65 is equivalent to a

~ 2.5 fold increase per 10 °C (i.e., $Q_{10} = 2.5$). Thus our modeled equation is:

Model 1: log(response) = B_0 + B_1 × (1/kT) + B_2 × log(red runner mass) +(1|mouse ID)

where B_0 is the intercept, B_1 is the thermal coefficient and estimate of E, B_2 is the coefficient associated with red runner mass, k is Boltzmann's constant at 8.617×10^{-5} eV/K, and T is temperature in Kelvins, and mouse ID is a random effect. Red runner mass was included for its theoretical significance and predictive value. Red runner mass, which varied fourfold, was strongly linked to red runner speed and time required for capture (Fig. S6). Additionally, the size of a red runner may reflect the difficulty of subduing it, as larger individuals may be harder to overpower.

In addition, we used corrected Akaike Information Criterion (AICc) to analyze the role of the following possible main predictor variables: mouse mass, mouse sex, trial number, day of trial, and order of heating/cooling trials. For random effects, we considered experimenter ID and the time-to-capture scorer ID in addition to mouse ID. We compared models using the AICc() and lmerTest::step() functions in R. Note that lmerTest::step uses backwards AIC selection. For all response variables, temperature, red runner mass, and mouse ID were associated with the lowest AIC values. Occasionally, for some response variables, mouse mass and trial number were part of the lowest AIC value. However, the value of the key parameter of interest — temperature — was insensitive to inclusion or exclusion of additional variables. For parsimony and ease of interpretation, reported results reflect only the variables shown in **Model 1**. All results, including permutations from adding additional variables, are reproducible using supplied code.

References

1. Hillebrand, H. On the generality of the latitudinal diversity gradient. *The American Naturalist* **163,** 192–211 (2004).
2. Raz, T. *et al.* Diversity gradients of terrestrial vertebrates–substantial variations about a common theme. *Journal of Zoology* **322,** 126–140 (2024).
3. Willig, M. R., Kaufman, D. M. & Stevens, R. D. Latitudinal gradients of biodiversity: pattern, process, scale, and synthesis. *Annual review of ecology, evolution, and systematics* **34,** 273–309 (2003).
4. Allen, A. P., Brown, J. H. & Gillooly, J. F. Global Biodiversity, biochemical Kinetics, and the energetic-equivalence rule. *Science* **297,** 1545–1548. ISSN: 1095-9203. `http://dx.doi.org/10.1126/science.1072380` (Aug. 2002).
5. Gillooly, J. F. & Allen, A. P. Linking global patterns in biodiversity to evolutionary dynamics using metabolic theory. *Ecology* **88,** 1890–1894 (2007).
6. Stegen, J. C., Enquist, B. J. & Ferriere, R. Advancing the metabolic theory of biodiversity. *Ecology letters* **12,** 1001–1015 (2009).
7. Buckley, L. B., Hurlbert, A. H. & Jetz, W. Broad-scale ecological implications of ectothermy and endothermy in changing environments. *Global Ecology and Biogeography* **21,** 873–885 (2012).
8. Storch, D. in *Metabolic ecology: a scaling approach* 120–131 (Wiley Online Library, 2012).
9. Gillooly, J. F., Brown, J. H., West, G. B., Savage, V. M. & Charnov, E. L. Effects of Size and Temperature on Metabolic Rate. *Science* **293,** 2248–2251. ISSN: 1095-9203. `http://dx.doi.org/10.1126/science.1061967` (Sept. 2001).
10. Caley, M. J. & Schluter, D. The relationship between local and regional diversity. *Ecology* **78,** 70–80 (1997).
11. Arita, H. T. & Rodríguez, P. Local-regional relationships and the geographical distribution of species. *Global Ecology and Biogeography* **13,** 15–21 (2004).
12. Belmaker, J. & Jetz, W. Regional pools and environmental controls of vertebrate richness. *The American Naturalist* **179,** 512–523 (2012).
13. Cairns, D., Gaston, A. & Huettmann, F. Endothermy, ectothermy and the global structure of marine vertebrate communities. *Marine Ecology Progress Series* **356,** 239–250. ISSN: 1616-1599. `http://dx.doi.org/10.3354/meps07286` (Mar. 2008).
14. Grady, J. M. *et al.* Metabolic asymmetry and the global diversity of marine predators. *Science* **363.** ISSN: 1095-9203. `http://dx.doi.org/10.1126/science.aat4220` (Jan. 2019).
15. Santini, L. *et al.* Global drivers of population density in terrestrial vertebrates. *Global Ecology and Biogeography* **27,** 968–979 (2018).
16. Kissling, W. D., Sekercioglu, C. H. & Jetz, W. Bird dietary guild richness across latitudes, environments and biogeographic regions. *Global Ecology and Biogeography* **21,** 328–340 (2012).
17. Kissling, W. D. *et al.* Establishing macroecological trait datasets: digitalization, extrapolation, and validation of diet preferences in terrestrial mammals worldwide. *Ecology and Evolution* **4,** 2913–2930 (2014).
18. Roslin, T. *et al.* Higher predation risk for insect prey at low latitudes and elevations. *Science* **356,** 742–744. ISSN: 1095-9203. `http://dx.doi.org/10.1126/science.aaj1631` (May 2017).

19. Burnside, W. R., Erhardt, E. B., Hammond, S. T. & Brown, J. H. Rates of biotic interactions scale predictably with temperature despite variation. *Oikos* **123,** 1449–1456 (2014).

20. O'Connor, M. P. *et al.* Reconsidering the mechanistic basis of the metabolic theory of ecology. *Oikos* **116,** 1058–1072 (2007).

21. Butler, K. Predatory behavior in laboratory mice: Strain and sex comparisons. *Journal of Comparative and Physiological Psychology* **85,** 243–249. ISSN: 0021-9940. `http://dx.doi.org/10.1037/h0035008` (1973).

22. Hoy, J. L., Yavorska, I., Wehr, M. & Niell, C. M. Vision Drives Accurate Approach Behavior during Prey Capture in Laboratory Mice. *Current Biology* **26,** 3046–3052. ISSN: 0960-9822. `http://dx.doi.org/10.1016/j.cub.2016.09.009` (Nov. 2016).

23. Hoy, J. L., Bishop, H. I. & Niell, C. M. Defined Cell Types in Superior Colliculus Make Distinct Contributions to Prey Capture Behavior in the Mouse. *Current Biology* **29,** 4130–4138.e5. ISSN: 0960-9822. `http://dx.doi.org/10.1016/j.cub.2019.10.017` (Dec. 2019).

24. Johnson, K. P. *et al.* Cell-type-specific binocular vision guides predation in mice. *Neuron* **109,** 1527–1539.e4. ISSN: 0896-6273. `http://dx.doi.org/10.1016/j.neuron.2021.03.010` (May 2021).

25. Dell, A. I., Pawar, S. & Savage, V. M. Systematic variation in the temperature dependence of physiological and ecological traits. *Proceedings of the National Academy of Sciences* **108,** 10591–10596. ISSN: 1091-6490. `http://dx.doi.org/10.1073/pnas.1015178108` (May 2011).

26. Eyring, V. *et al.* Overview of the Coupled Model Intercomparison Project Phase 6 (CMIP6) experimental design and organization. *Geoscientific Model Development* **9,** 1937–1958 (2016).

27. Riahi, K. *et al.* The Shared Socioeconomic Pathways and their energy, land use, and greenhouse gas emissions implications: An overview. *Global environmental change* **42,** 153–168 (2017).

28. Danabasoglu, G. *NCAR CESM2 model output prepared for CMIP6 ScenarioMIP ssp126* 2019. `https://doi.org/10.22033/ESGF/CMIP6.7746`.

29. Danabasoglu, G. *NCAR CESM2 model output prepared for CMIP6 ScenarioMIP ssp245* 2019. `https://doi.org/10.22033/ESGF/CMIP6.7748`.

30. Danabasoglu, G. *NCAR CESM2 model output prepared for CMIP6 ScenarioMIP ssp585* 2019. `https://doi.org/10.22033/ESGF/CMIP6.7768`.

31. Tittensor, D. P. *et al.* Global patterns and predictors of marine biodiversity across taxa. *Nature* **466,** 1098–1101 (2010).

32. Schemske, D. W., Mittelbach, G. G., Cornell, H. V., Sobel, J. M. & Roy, K. Is there a latitudinal gradient in the importance of biotic interactions? *Annu. Rev. Ecol. Evol. Syst.* **40,** 245–269 (2009).

33. LaManna, J. A. *et al.* Plant diversity increases with the strength of negative density dependence at the global scale. *Science* **356,** 1389–1392 (2017).

34. Paquette, A. & Hargreaves, A. L. Biotic interactions are more often important at species' warm versus cool range edges. *Ecology Letters* **24,** 2427–2438 (2021).

35. Hertz, P. E., Huey, R. B. & Nevo, E. Fight versus flight: body temperature influences defensive responses of lizards. *Animal Behaviour* **30,** 676–679 (1982).

36. Rand, A. S. Inverse relationship between temperature and shyness in the lizard Anolis lineatopus. *Ecology* **45,** 863–864 (1964).

37. Hurlbert, A. H., Ballantyne, F. & Powell, S. Shaking a leg and hot to trot: the effects of body size and temperature on running speed in ants. *Ecological Entomology* (2008).

38. Vogel, P. in *Comparative physiology: Primitive mammals* (eds Schmidt-Nielsen, K., Bolis, L. & Taylor, C. R.) 170–180 (Cambridge University Press, 1980).

39. He, J., Tu, J., Yu, J. & Jiang, H. A global assessment of Bergmann's rule in mammals and birds. *Global Change Biology* **29,** 5199–5210 (2023).

40. Pincheira-Donoso, D. & Meiri, S. An intercontinental analysis of climate-driven body size clines in reptiles: no support for patterns, no signals of processes. *Evolutionary Biology* **40,** 562–578 (2013).

41. Smith, F. A. *et al.* Body size evolution across the Geozoic. *Annual Review of Earth and Planetary Sciences* **44,** 523–553 (2016).

42. Londoño, G. A., Gomez, J. P., Sánchez-Martínez, M. A., Levey, D. J. & Robinson, S. K. Changing patterns of nest predation and predator communities along a tropical elevation gradient. *Ecology Letters* **26,** 609–620 (2023).

43. Damuth, J. Population density and body size in mammals. *Nature* **290,** 699–700 (1981).

44. IUCN. 2021.

45. *Bird species distribution maps of the world* 2017.

46. Roll, U. *et al.* The global distribution of tetrapods reveals a need for targeted reptile conservation. *Nature ecology & evolution* **1,** 1677–1682 (2017).

47. Zhang, D. *rsq: R-Squared and Related Measures* R package version 2.6 (2023). `https://CRAN.R-project.org/package=rsq`.

48. Riebler, A., Sørbye, S. H., Simpson, D. & Rue, H. An intuitive Bayesian spatial model for disease mapping that accounts for scaling. *Statistical methods in medical research* **25,** 1145–1165 (2016).

49. Rue, H., Martino, S. & Chopin, N. Approximate Bayesian inference for latent Gaussian models by using integrated nested Laplace approximations. *Journal of the Royal Statistical Society Series B: Statistical Methodology* **71,** 319–392 (2009).

50. Mathis, A. *et al.* DeepLabCut: markerless pose estimation of user-defined body parts with deep learning. *Nature neuroscience* **21,** 1281–1289 (2018).